THE SIMULATION OF WHOLE CORE PERMEAMETER FLOW GEOMETRY

A Thesis

Submitted to the Graduate Faculty of the
Louisiana State University and
Agricultural and Mechanical College
in partial fulfillment of the
requirements for the degree of
Master of Science

in

The Department of Petroleum Engineering

by
Louis Oved Chemin, Jr.
B.S., Louisiana State University, 1973
August, 1974

ACKNOWLEDGMENT

The author wishes to express gratitude to Dr. William R. Holden, Professor of Petroleum Engineering, under whose direction this research was conducted; to Dr. A. T. Bourgoyne, Jr., Associate Professor of Petroleum Engineering, and Dr. O. K. Kimbler, Professor of Petroleum Engineering, for their encouraging, helpful, and timely suggestions.

This work was financed in part by a Federal grant under PL 88-379, administered by the Louisiana Water Resources Research Institute with funding from the Office of Water Resources Research, U.S. Department of the Interior, projects A-023-LA and A-032-LA. The author also wishes to express gratitude to the Gulf Oil Foundation for the award of the Gulf Graduate Fellowship in the Department of Petroleum Engineering during the academic year 1973-74. All computations were made by use of the IBM 360 computer Varian plotter at the Computer Research Center of Louisiana State University.

The author's sincere appreciation is extended to his wife, Mrs. Marilyn Chemin, and Mrs. Mary Matens for typing this manuscript.

Finally, the author dedicates this work to his parents for their having impressed upon him the value of education and for their faithful encouragement.

TABLE OF CONTENTS

TABLE OF CONTENTS (CONTINUED)

LIST OF TABLES

LIST OF FIGURES

LIST OF FIGURES (CONTINUED)

LIST OF FIGURES (CONTINUED)

ABSTRACT

Numerous studies of fluid flow in porous media have shown that sedimentary formations do not always conduct fluids equally well in all directions in the plane of bedding. This characteristic of preferential directions of flow is referred to as anisotropic or directional permeability. Various laboratory techniques have been developed to obtain anisotropic permeability data from core samples. One of the more sophisticated techniques employs an apparatus known as a whole core permeameter. At the present time, however, this permeameter is primarily used to analyze isotropic cores whose permeability is not direction sensitive. The necessary analytical description of the flow field within the permeameter has yet to be developed for the case of an anisotropic core.

Reported in this work are the results of various attempts to simulate this complex flow geometry by means of two different types of mathematical models — a finite element model and an image well and streamline model.

CHAPTER I

Introduction

The problems of meeting the world's needs in the areas of energy production, waste disposal, gas storage, fresh water storage, etc., has resulted in an effort to better define and predict reservoir properties. Presently the Petroleum Industry is spending millions of dollars on reservoir simulators which help to predict reservoir performance with respect to fluid migration, production capacities, pressure distributions, and boundary locations and characteristics. These predictive calculations are made in order to perform an economic analysis on a project before it is undertaken. However, in spite of the great advances made in the development of complex reservoir models, many uneconomical projects are erroneously undertaken as a result of inaccurate predictions. Reservoir inhomogeneity and anisotropy have often been cited as two reasons for such inaccuracies.

Reservoir inhomogeneity results from several phenomena. One phenomenon is the lateral changes in permeability due to a sedimentary facies change. This occurs when some geological event disrupts the continuous process of deposition and cementation. Stratification is a second phenomenon contributing to reservoir inhomogeneity with an associated change in vertical permeability. In addition

there is another phenomenon to be considered called anisotropic permeability. Engineering studies of fluid flow in porous media have often pointed out that sedimentary formations do not always conduct fluids equally well in all directions in the plane of bedding. This characteristic of preferential directions of flow is what is referred to as anisotropic or directional permeability.

Reservoir models have been developed and are being used daily that will handle these problems of inhomogeneity and anisotropy. Some models handle them by allowing the isotropic or anisotropic permeability of finite reservoir blocks to be specified as a function of flow direction along the x, y, and z axes. Other models make use of clever axes transformations in the equations of flow to accommodate permeability anisotropy. However, these sophisticated models are only as accurate as the input data which defines the characteristics of the reservoir to be simulated.

Over the years various laboratory techniques have been developed to obtain permeability data from core samples. Several of these techniques will be discussed in detail in the next chapter. One of the more sophisticated techniques is the use of what is commonly known as a "whole core permeameter." This apparatus can be used to non-destructively analyze core samples ranging from 2-3/4 to 5-3/8 inches in diameter and 2 to 20 inches in length. The permeameter consists of small coil springs or screen

applied longitudinally to opposite sides of the core exposing those areas to flow. The remainder of the core is sealed by a rubber sleeve under pressure and two thick rubber end plugs. Attached to the rubber sleeve adjacent to the areas open to flow are two rigid tubes which extend through the metal cylinder in which the apparatus is contained. Flow enters through one tube, traverses the core and exits by the opposite tube (see Figure 1-1). The flow rate and difference in potential across the core are monitored to allow the calculation of permeability.

As can be seen in Figure 1-1, the flow geometry of the whole core permeameter is quite complex. Collins[2] derived an analytical solution for this flow geometry for the case of an isotropic and homogeneous core sample. He found that the magnitude of the flow which traverses an isotropic core is a function of the angle, α, open to flow, the potential difference across the core, the fluid viscosity, the isotropic permeability, and the length of the core. At present, the whole core permeameter is also used to qualitatively study anisotropic core samples. This is accomplished by rotating the core sample in the rubber sleeve until the unique orientations for both maximum and minimum flow rates have been observed for a given pressure drop across the system. This defines the orientations of the major and minor axes of permeability. The permeability associated with flow parallel to the major

axis is denoted as K_x and is in the direction in which the maximum flow rate is realized. Likewise, the permeability associated with flow parallel to the minor axis is denoted as K_y and is in the direction in which the minimum flow rate is realized. The anisotropy ratio, A, is defined as K_x/K_y, where $K_x > K_y$. As previously mentioned, the orientation of the major and minor axes can be found by rotating the core in the permeameter, but at present there is no technique available to evaluate the magnitude of the principal permeability values, K_x and K_y. From Collins' work, however, it is believed that the magnitude of flow for an anisotropic core would be, in addition to the previously mentioned parameters, a function of the anisotropy ratio, A, and the orientation of the major and minor axes of permeability with respect to the areas open to flow.

Even under the ideal condition of isotropic permeability the flow geometry of the permeameter system is quite complex. With the addition of anisotropy this complexity increases such that a solution similar to that of Collins' for the isotropic case would seem to be extremely difficult. An analytical solution by some form of axis transformation would be complicated further as the core must be tested for various orientations of the principal axes. Therefore, the purpose of this study was to numerically simulate the flow geometry of the whole core permeameter under isotropic and anisotropic

conditions to determine the effects of the size of angular openings exposed to flow, various orientations of the principal axes of permeability, and different anisotropy ratios.

CHAPTER II

Previous Investigations

2.1 Review of Studies on Anisotropy

Fettke[4] observed the phenomenon of directional permeability in 1938 while analyzing samples of Bradford sandstone. In his study to determine an average permeability he took 63 cubic samples and measured their permeabilities in two horizontal directions. Even though two opposite faces of a cube were aligned with the bedding plane, Fettke made no attempt to determine the orientation of the axes of permeability in the bedding plane itself. The maximum horizontal permeability ratio observed by Fettke was 1.77.

Pettijohn[14] has pointed out that sedimentary formations will usually exhibit a larger fluid conductivity for flow along the plane of bedding as compared with flow perpendicular to the plane of bedding. In addition to Pettijohn, Johnson and Hughs[8] and Greenkorn[5], et al., indicated that nearly all sedimentary formations, when considering two-dimensional flow in the plan of bedding, exhibit preferred directions of flow.

In the literature reviewed by Holden[6] in his study of permeability microstratification in natural sandstones, he found that for homogeneous sandstones the anisotropy ratio is less than 2.0.

Hutchinson[7] reported an average ratio of 16.0 while analyzing limestone cores. Values higher than 16.0 have been observed in fractured formations such as the Spraberry trend where values as high as 144.0 have been reported.

When planning secondary or tertiary recovery projects the effects of anisotropic permeability must be considered. To support this idea Landrum and Crawford[10] and Mortada and Nabor[12] conducted studies to determine the sweep efficiency and flow capacities of a number of well pattern geometries to include the effects of anisotropic permeability. In addition, Johnson and Hughs[8] and Barfield[1], et al., suggested functional relationships between optimum injection well locations and the principal directions of permeability. These studies indicate, that without considering anisotropic permeability when selecting injection and production well locations, problems such as poor sweep efficiency, premature breakthrough and loss of otherwise recoverable hydrocarbons may occur.

Kelton[9], Collins[2], and Rinard[15] have also made contributions to the study of anisotropy. Their findings along with those of Johnson and Hughs are discussed in more detail in the next section.

2.2 Laboratory Techniques to Measure Anisotropic Permeability

Several techniques have been developed over the years to measure isotropic as well as anisotropic

permeability. These techniques can be characterized by their flow geometry.

2.2a Linear Technique

Johnson and Hughs[8] developed two techniques to measure the anisotropy of core samples. The first technique was based on linear flow measurements. It involved a 2-1/4-inch O.D. by 2.0 or 3.0-inch long diamond core sample, faced on both ends, and marked with a longitudinal orientation line along the side. The sample was then cut into disks about 1/4-inch thick. Each disk was then cut into 8 small plugs oriented 45 degrees apart. The plugs were 1/4-inch wide (see Figure 2-1). Air permeability measurements were then made on each linear plug and recorded. The permeabilities for each disk were normalized by setting the maximum permeability equal to 100%. These values were then plotted on polar co-ordinate paper thus showing the orientation of the major and minor axes of permeability.

2.2b Radial Technique

The second technique developed by Johnson and Hughs[8] was based on radial flow. It involved small diamond core samples as previously described with a hole approximately 1.0-centimeter in diameter drilled longitudinally through the center. The test apparatus consisted of a system of clamps mounted with bearings which allowed the sample to

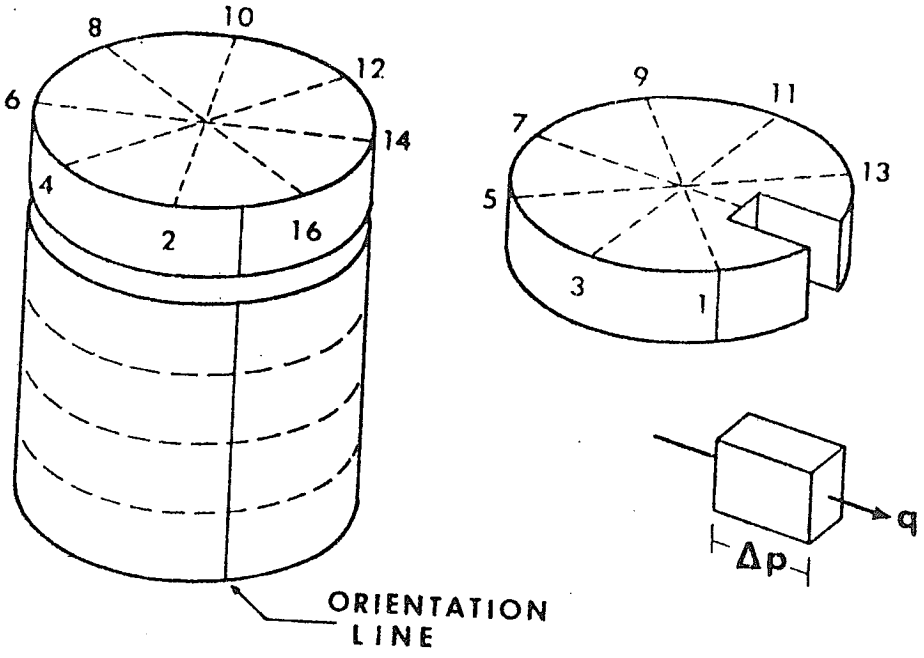

FIGURE 2-1 SAMPLING PLAN FOR ORIENTED CORE PLUGS USED IN DIRECTIONAL FLOW TESTS. (After Holden[6], Ph.D. Dissertation.)

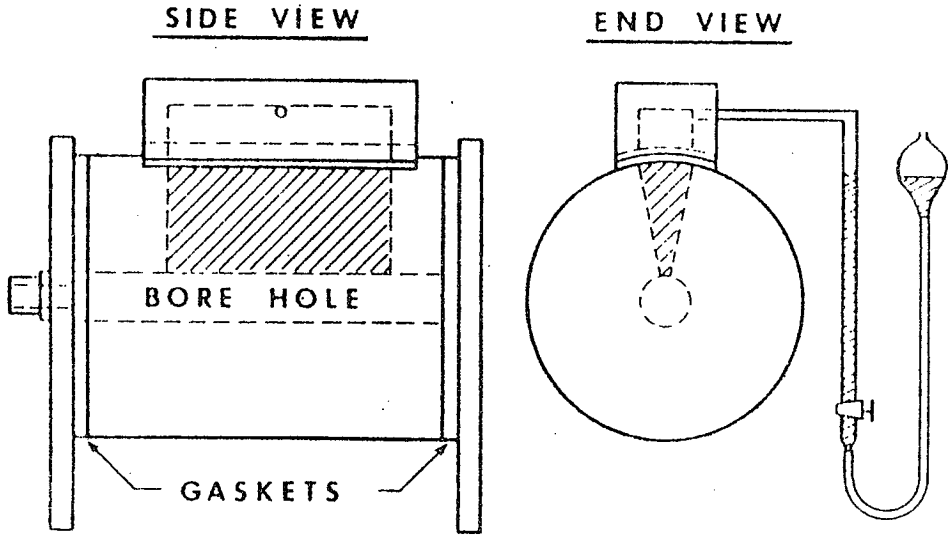

FIGURE 2-2 SCHEMATIC DRAWING OF DIRECTIONAL FLOW PERMEAMETER. (After Holden[6], Ph.D. Dissertation.)

be rotated to any position for flow measurements while gas was injected at a constant rate through the center hole. The radial flow was monitored by a collecting head clamped to the side of the sample. Air permeability measurements were then made on 30-degree intervals around the sample (see Figure 2-2). These values were also normalized and plotted on polar co-ordinate paper.

2.2c Spherical Technique

Holden[6] developed a technique to observe inhomogeneities and anisotropy in sandstones based on spherical flow. The technique consisted of bonding a plastic mandrel on one face of a sandstone sample which had been cut parallel to its bedding plane. A 1/4-inch hole was bored through the mandrel partially into the rock creating a hemispherical cavity open to flow. The rock sample was then machined into a 4-inch diameter hemisphere by means of a lathe. The sample was saturated with and submerged in a bath of clear naphtha, to eliminate all effects of gravity.

A red-dyed naphtha was injected into the center of the hemisphere and its breakthrough on the outer surface was monitored by means of a camera and mirror combination (see Figure 2-3). The results of this spherical technique revealed that for the limited number of sandstones tested the flow was mainly along the bedding planes, with little evidence of anisotropy.

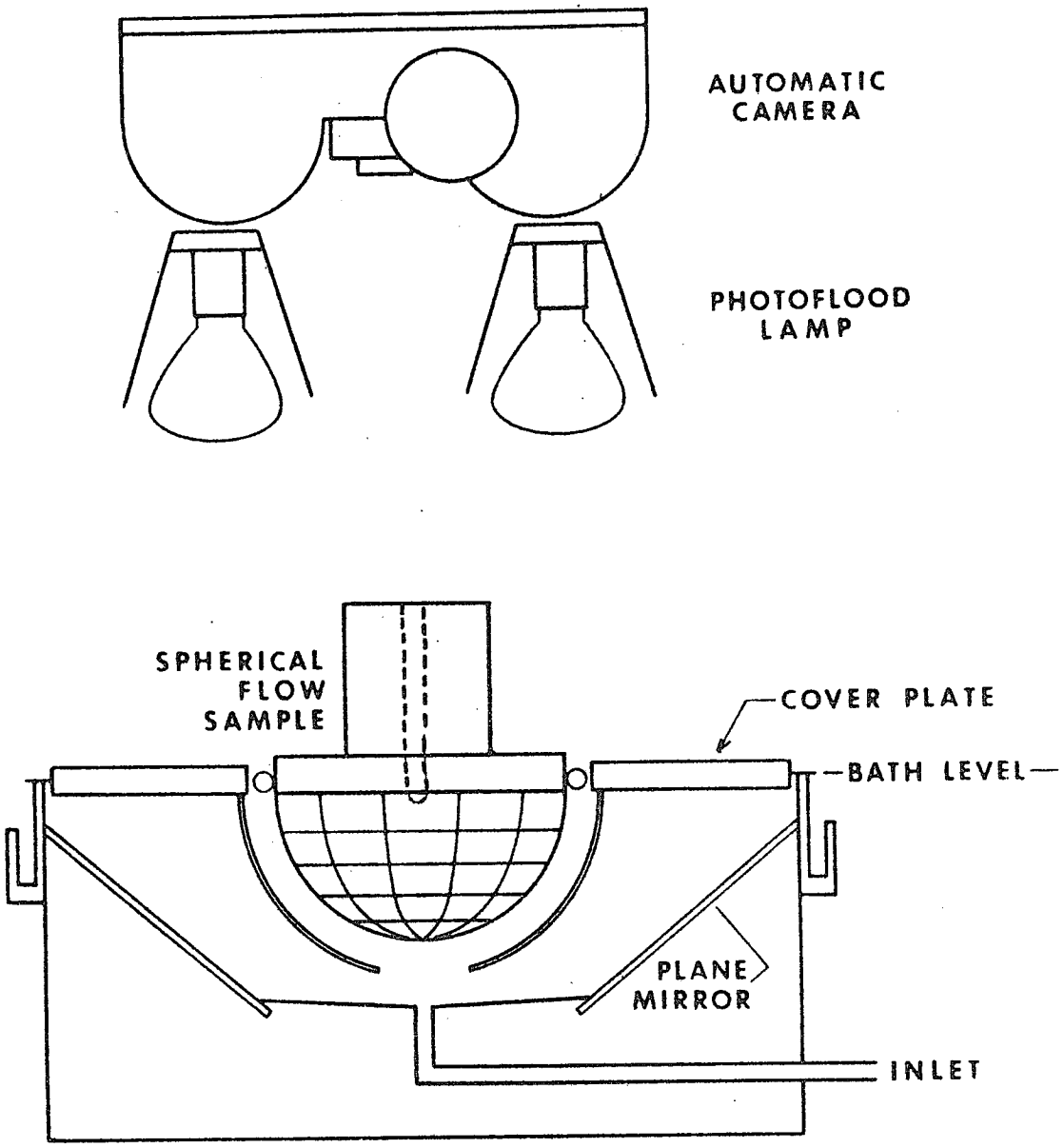

FIGURE 2-3 SCHEMATIC DRAWING OF THE SPHERICAL FLOW APPARATUS.
(After Holden[6], Ph.D. Dissertation.)

2.2d Whole Core Permeameter Techniques

There have been at least three independent studies conducted by Kelton, Collins, and Rinard on flow geometry of the whole core permeameter.

In 1949 Kelton described an apparatus similar to the conventional whole core permeameter. His clamp type device consisted of two rubber gaskets with rectangular openings in the centers which extended approximately the full length of the core. These gaskets were clamped to the core by two sections of split pipe thus sealing the core with the exception of the gasket openings, the ends, and a thin line along the side of the core between the gaskets (see Figure 2-4). Air permeability calculations were made which incorporated correction factors for the effects of non-linear flow, various size gasket openings, and leakage from the ends of the core and the lines between the gaskets.

These correction factors were derived from the study of a synthetic core of nearly uniform permeability with different gasket openings and core lengths. A subsequent check was made by use of an electrolytic model, simulating the non-linear flow through the core. This technique, however, is applicable only to the analysis of isotropic core samples.

As previously mentioned, Collins derived an analytical solution to the isotropic flow geometry of the conventional

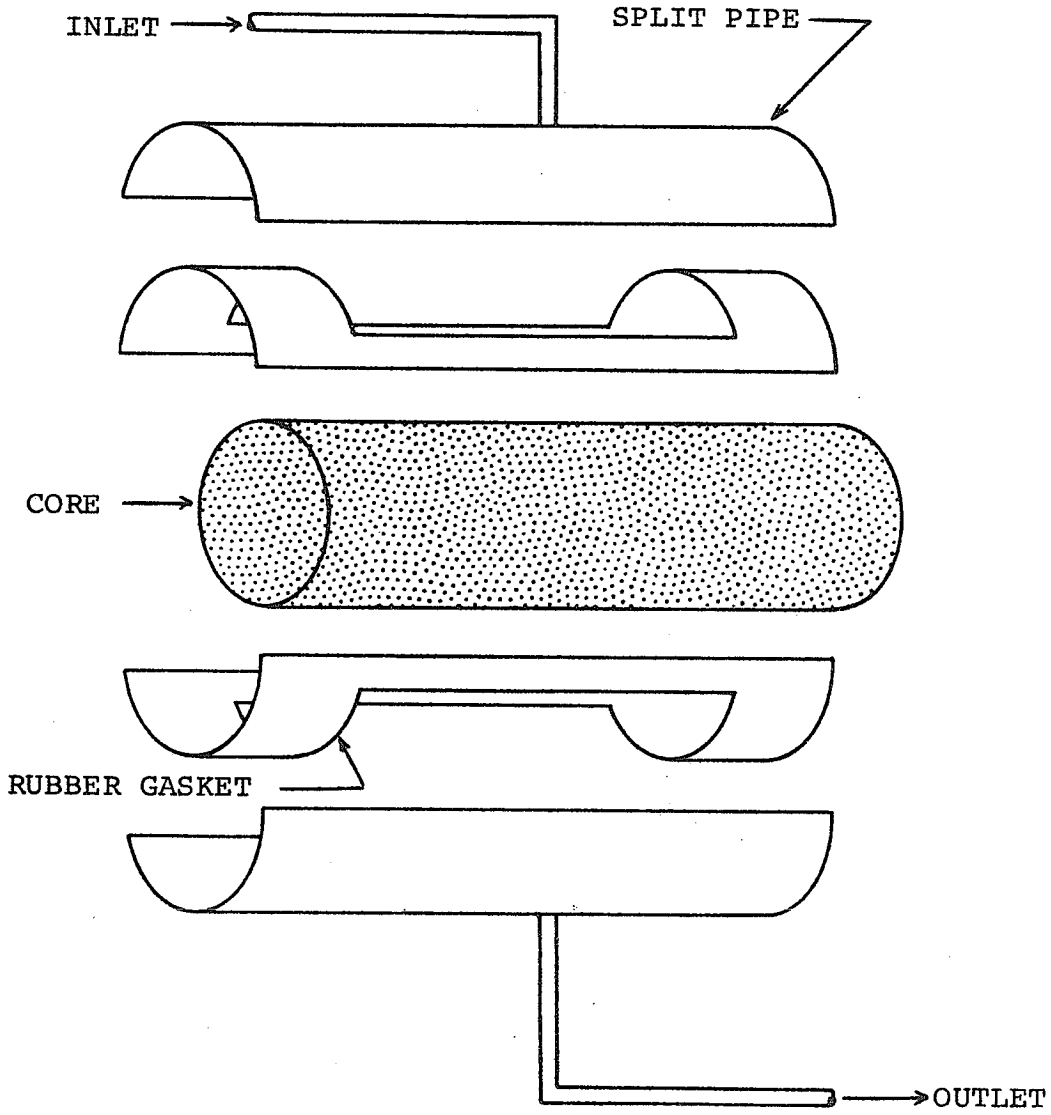

FIGURE 2-4 SCHEMATIC DRAWING OF CLAMP-TYPE PERMEAMETER. (After Kelton[9], TRANS. AIME.)

whole core permeameter. His solution involved the use of the steady state form of Laplace's equation for two dimensional flow:

$$\frac{\partial^2 p}{\partial x^2} + \frac{\partial^2 p}{\partial y^2} = 0 \qquad (2.1)$$

and a series of conformal mapping transformations. A geometric factor, G, was derived to correct for the effects of the non-linear flow. This geometric factor is a function of one-half the angle, α, open to flow (see Figure 1-1) and appears in the following equation:

$$K = \frac{\mu q}{L\Delta p} \cdot G(\alpha) \qquad (2.2)$$

which is the integrated form of Darcy's law describing isotropic traverse flow in a whole core permeameter. α is one-half of the angle open to flow, K is the isotropic permeability, μ is the fluid viscosity, L is the length of the area open to flow, q is the flow rate across the core, Δp is the potential difference, and $G(\alpha)$ is the geometric factor. For a plot of the geometric factor versus the half-angle opening see Figure 2.5.

Rinard, in an effort to simulate both isotropic and an anisotropic flow in a whole core permeameter, verfied Collins' work on isotropic flow and developed some empirical correction factor curves for anisotropic flow. His electrical analog of porous media consisted of a series of electrically conductive grids, drawn with

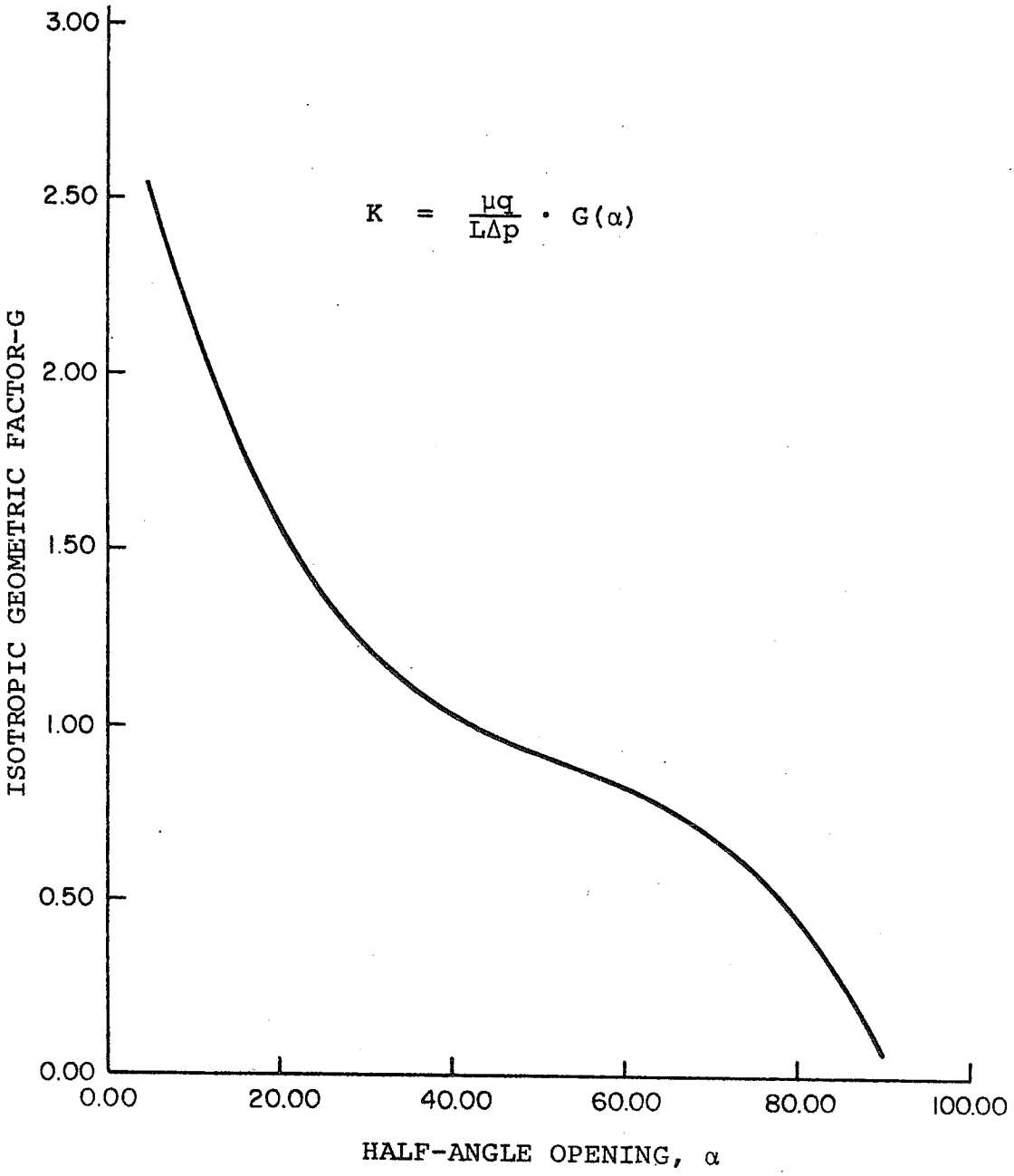

FIGURE 2-5 COLLINS' GEOMETRIC FACTOR FOR INTERPRETATION OF ISOTROPIC WHOLE CORE PERMEAMETER MEASUREMENTS.

conductive ink on mylar film. For the isotropic system the grid lines were of uniform breath and equally spaced to produce a repetitive square pattern. An anisotropic system was constructed such that the common distance between the parallel lines in the X-direction was less than the distance between the lines in the Y-direction, where the X and Y-directions are orthogonal. This resulted in more lines available to current flow in the X-direction. Hence, the conductivity in the X-direction was a maximum which corresponded to a principal value of maximum permeability. Each grid was cut into a circle to simulate the geometry of a core sample.

His electrical analog of the permeameter was made of a circular disk of plexyglass with a strip of highly conductive rubber inlaid around the outer perimeter (see Figure 2-6). Variations in the angle open to flow were accomplished by reducing the lengths of the conductive rubber electrodes. To simulate various orientations of the principal axes the grids were rotated in 5-degree increments.

Rinard concluded that the geometric factor for traverse flow under anisotropic conditions was not only a function of angle opening but of the anisotropy ratio and orientation of the principal axes as well. He proposed a modified form of Collins' equation describing two dimensional flow in an anisotropic whole core permeameter system

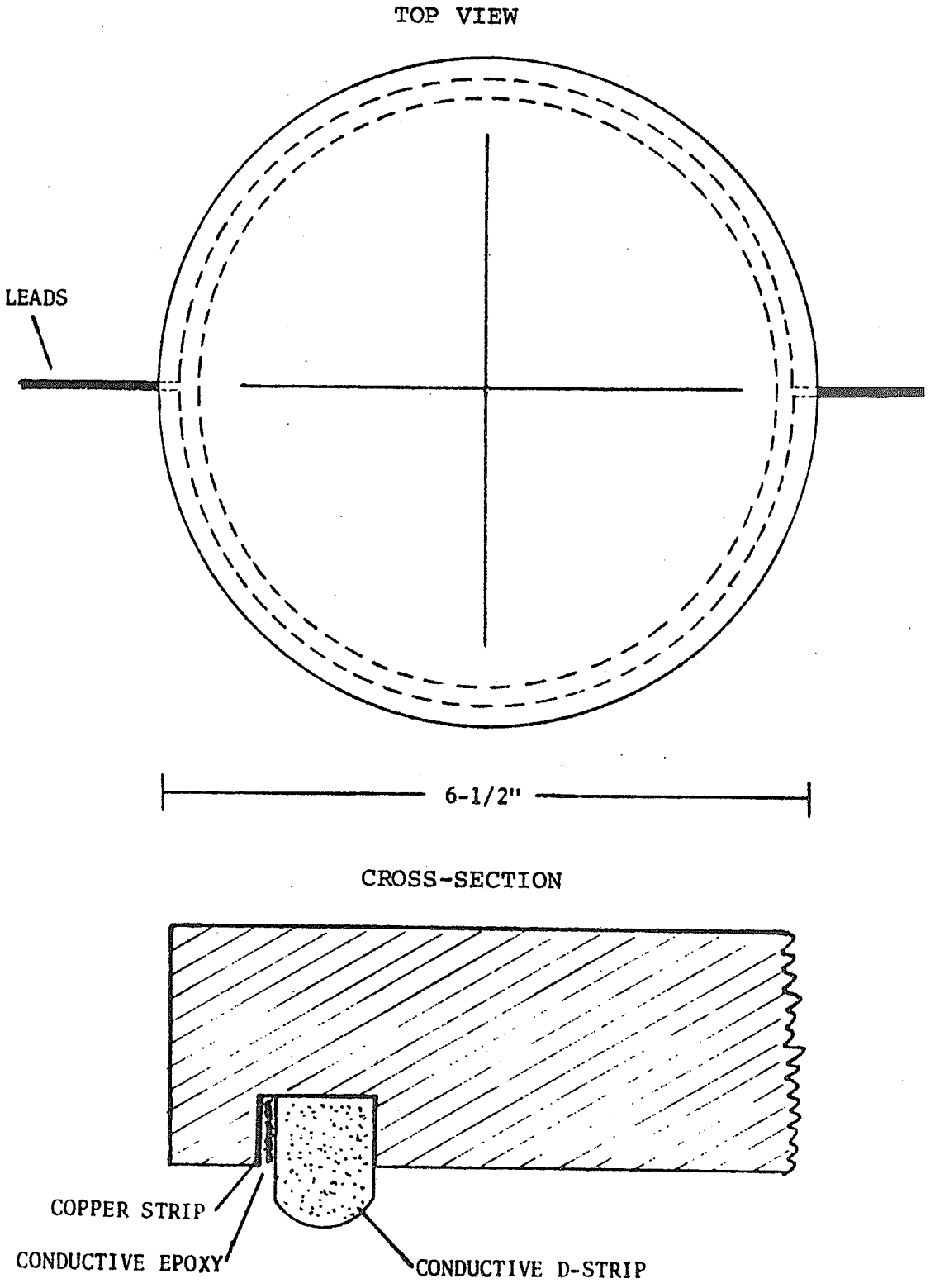

FIGURE 2-6 SCHEMATIC OF CONTACT ELECTRODE USED IN PERMEAMETER ANALOG. (After Rinard[15], M.S. Thesis.)

as:

$$K_{max} = \frac{\mu\, q_{max}}{L\Delta p} \cdot G(\alpha, A, 0°) \qquad (2.3)$$

where K_{max} is the principal permeability along the major axis, q_{max} is the maximum flow rate experienced when the major axis is oriented at 0 degrees with respect to the areas open to flow, and $G(\alpha, A, 0°)$ is the geometric factor for a half-angle of α, an anisotropy ratio of A, and with the orientation of the major axis at 0 degrees.

CHAPTER III

Flow Geometry and Model Selection

3.1 Description of Flow Geometry

The complexity of the flow geometry and boundary conditions of the whole core permeameter made the selection and adaptation of a proper mathematical simulator rather difficult. These boundary conditions and flow geometry can best be described by referring to Figure 3-1. The boundaries B and B' are no-flow boundaries. They are imposed on the system when the core is partially sealed by the rubber sleeve under pressure. Boundaries A and A' are isopotential boundaries and are imposed on the system when fluid is injected over the entire angle opening. The potential at boundary A must be greater than the potential at boundary A'. The influx and efflux must cross these isopotential boundaries at right angles for the case of isotropic flow. In addition, there are four points of discontinuity C_1, C_2, C_3, and C_4. These points are formed by the abrupt connections between the no-flow boundaries and the isopotentials.

For the isotropic conditions the streamline pattern is intuitively represented as in Figure 3-1. However, for anisotropic conditions the pattern is believed to be more complicated and dependent upon the anisotropy ratio and the orientation of the major and minor axes of permeability.

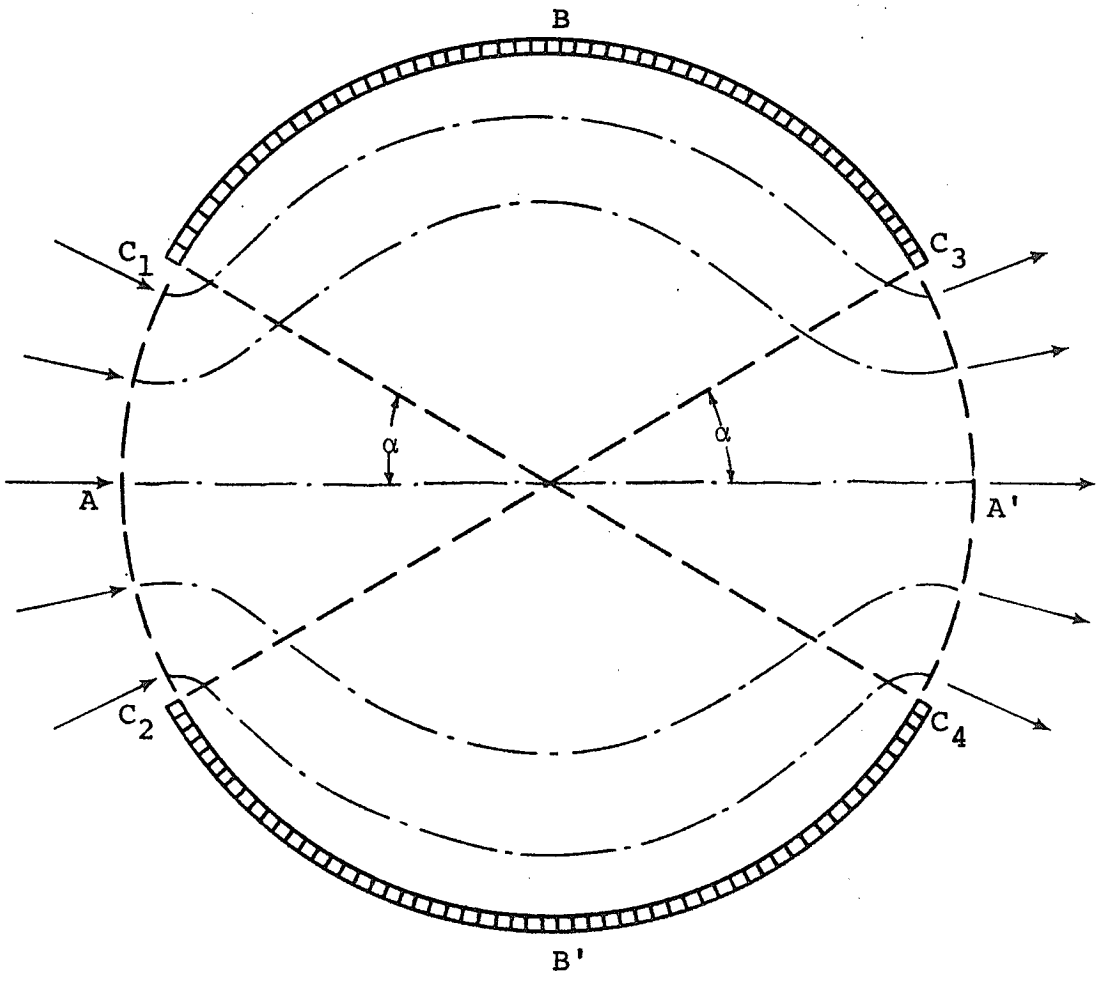

FIGURE 3-1 INITUITIVE STREAMLINE PATTERN FOR THE ISOTROPIC FLOW GEOMETRY OF THE WHOLE CORE PERMEAMETER, SHOWING HALF-ANGLE OPENING, α.

3.2 Finite Element Model by Cooley and Peters

In 1970 Cooley and Peters[3], while working for the U.S. Hydraulic Engineering Center, developed a finite element model that was primarily designed to handle problems involving single phase, steady state, two dimensional or axisymmetric flow in heterogeneous anisotropic porous media. In particular, the program was developed to analyze ground water and seepage problems but supposedly was applicable to potential flow problems of any type.

The theory behind the finite element model is similar to that of other models in that it deals with the following physical principles:

1. Law of Conservation of Mass (flow)
2. Darcy's Law
3. An Equation of State

The conservation of mass for steady state incompressible fluid in two dimensional flow was expressed as:

$$W(x,y) = -\left[\frac{\partial V_x}{\partial x} \cdot m + \frac{\partial V_y}{\partial y} \cdot m\right] \qquad (3.1)$$

where V_x and V_y are the apparent velocities or discharge per unit area in the X and Y-directions respectively, m is the thickness, and W(x,y) is the discharge per unit area of a source or sink term. The source terms are negative while the sink terms are positive.

Darcy's law for steady state, two dimensional laminar flow was of the form:

$$V_x = \frac{-K_x}{\mu} \frac{\partial \Phi}{\partial x}; \quad V_y = \frac{-K_y}{\mu} \frac{\partial \Phi}{\partial y}$$

where μ is the fluid viscosity, K_x and K_y are the permeabilities in the X and Y-directions which correspond to the major and minor axes respectively, and $\frac{\partial \Phi}{\partial x}$ and $\frac{\partial \Phi}{\partial y}$ are the components of the potential gradient in the X and Y-directions.

The basic flow equation solved by the model was a combination of the continuity equation and Darcy's law expressed as:

$$W(x,y) = \frac{\partial}{\partial x} \left[\frac{K_x}{\mu} \cdot m \cdot \frac{\partial \Phi}{\partial x}\right] + \frac{\partial}{\partial y} \left[\frac{K_y}{\mu} \cdot m \cdot \frac{\partial \Phi}{\partial y}\right] \quad (3.3)$$

The model was also designed to transform cartesian co-ordinates, (x,y) into axisymmetrical co-ordinates, (r,z) to solve the following flow equation for cylindrical flow:

$$\frac{1}{r} \frac{\partial}{\partial r} \left[K_r \cdot r \frac{\partial \Phi}{\partial r}\right] + \frac{\partial}{\partial z} \left[K_z \frac{\partial \Phi}{\partial z}\right] = 0 \quad (3.4)$$

Since the partial differential equations were solved by the finite element method it should be noted that the orientation and magnitude of the principal axes of permeability did not have to be constant throughout the entire flow region-but only in each element. This enabled the model to be used to study inhomogeneous anisotropic problems.

The model was designed such that the flow region was to be divided into quadrilateral elements with the corners,

referred to as nodes, being the points at which the potential function was evaluated. There were no restrictions as to the actual size or shape of the elements other than they had to contain four nodes. This feature led to the development of a grid system that could be weighted with detail in the areas of discontinuity without having to extend the same detail over the entire system.

The boundary conditions that could be modeled were those of isopotential boundaries, no-flow boundaries, and boundaries of steady state influx or efflux. The no-flow boundaries could be simulated by specifying a flux of zero across the element faces falling on the no-flow boundaries. Likewise, the isopotential boundaries could be simulated by assigning a common potential to all nodes on the isopotentials. Concerning those areas of discontinuity in a whole core permeameter system, since the size and shape of the quadrilateral elements were not restricted, it was felt that enough definition could be obtained in those areas by a suitable choice of small elements without having to propagate this same detail throughout the entire flow region, thus reducing computer time and expense.

Another requirement was the simulation of not only an isotropic system but one of an anisotropic nature. As previously mentioned, this model was so designed that each individual element in the flow region could be specified, completely independent of its neighbor, with its own

orientation and magnitudes for the principal values of permeability.

3.3 Image Well and Streamline Model

In 1972 Lin[11] employed a technique of using image wells to bound arbitrary reservoir shapes. This technique utilized the potential distribution about a single well in an infinite system as defined by what is commonly called the line source equation. In addition it involved the principle of superimposing the potentials from a series of image wells and the tracking of the resulting streamlines.

3.3a Basic Equations

The line source equation was derived by applying the same three physical principles mentioned in Section 3.2 for a single well in an infinite homogeneous isotropic system. The potential, Φ, at some point, (x_j,y_j), was expressed as:

$$\Phi(x_j,y_j) = \frac{-\mu q_i}{4\pi kh} \cdot \ln\left[(x_j-x_i)^2 + (y_j-y_i)^2\right] + C \quad (3.5)$$

where q_i/h is the strength of the line source located at the point (x_i,y_i). By applying the technique of superposition to accomodate a multiwell system, equation (3.5) expands to:

$$\Phi(x_j,y_j) = \frac{-\mu}{4\pi kh} \sum_{i=1}^{N} q_i \cdot \ln\left[(x_j-x_i)^2 + (y_j-y_i)^2\right] + C \quad (3.6)$$

where N is the number of wells in the system and C is an arbitrary constant. It should be noted that this equation is for a set of consistant units and that the strength of all production wells must be negative, while all injection wells must be positive.

For anisotropic conditions equation (3.6) becomes:

$$\Phi(x_j,y_j) = \frac{-\mu}{4\pi h\sqrt{k_x k_y}} \cdot \sum_{i=1}^{N} q_i \ln\left[\frac{(x_j-x_i)^2}{k_x} + \frac{(y_j-y_i)^2}{k_y}\right]+C \qquad (3.7)$$

The potential gradient components in the X and Y-directions were obtained by differentiating Equation (3.7):

$$\frac{\partial\Phi}{\partial x}\Big|_j = \frac{-\mu k_y}{2\pi h\sqrt{k_x k_y}} \cdot \sum_{i=1}^{N} q_i \left[\frac{(x_j-x_i)}{k_y(x_j-x_i)^2+k_x(y_j-y_i)^2}\right] \qquad (3.8a)$$

$$\frac{\partial\Phi}{\partial y}\Big|_j = \frac{-\mu k_y}{2\pi h\sqrt{k_x k_y}} \cdot \sum_{i=1}^{N} q_i \left[\frac{(y_j-y_i)}{k_y(x_j-x_i)^2+k_x(y_j-y_i)^2}\right] \qquad (3.8b)$$

The components of the apparent velocity at the point (x_j,y_j) were expressed as:

$$V_{xj} = \frac{-K_x}{\mu\phi_d} \cdot \frac{\partial\Phi}{\partial x}\Big|_j \qquad (3.9a)$$

$$V_{yj} = \frac{-K_y}{\mu\phi_d} \cdot \frac{\partial\Phi}{\partial y}\Big|_j \qquad (3.9b)$$

where ϕ_d is the displacable porosity.

The resultant apparent velocity was then:

$$V_{T_j} = \sqrt{V_{xj}^2 + V_{yj}^2} \qquad (3.10)$$

Assuming that V_{T_j} remained constant over a small distance, the time required to move a distance, ΔS, from a point (X_j, Y_j) was expressed as:

$$t_j = \frac{\Delta S}{V_{T_j}} \tag{3.11}$$

The new location of a fluid particle was expressed by:

$$X_{j+1} = X_j + V_{xj} \cdot t_j \tag{3.12a}$$

$$Y_{j+1} = Y_j + V_{xj} \cdot t_j \tag{3.12b}$$

By applying Equations (3.8a) through (3.12b) in an interative manner he was able to track individual streamlines. This same sequence of equations may also be applied to an isopropic system, where $K_x = K_y$.

3.3b No-Flow Boundary Simulation

For an isopropic system, at any point on a no-flow boundary the component of the potential gradient normal to the boundary must be zero. Lin approximated this requirement in the following steps:

1. Specifying the locations for a system of N image wells distributed in a somewhat uniform manner beyond the periphery of the flow region to be bounded.

2. Specifying the locations of m pairs of points which straddle the desired no-flow boundary. The members of a given pair define the end points of an imaginary line segment which is normal to and bisected by the boundary.

3. Adjusting the strengths of the image wells considered in Step 1 so that the potentials enjoyed by each point in a given pair are equal.

A test of whether or not a no-flow boundary was realized was made by tracking streamlines near the desired no-flow boundary. Applying Equation (3.6) to each of the boundary pairs produced a series of m linear equations in N unknowns which were solved by matrix transposition and Gauss elimination.

3.3c Isopotential Boundary Simulation

In the simulation of an isopotential boundary a similar line of logic was used. The idea was to specify a series of points lying on the desired boundary and by means of Equation (3.6) require that all points enjoy the same potential.

3.3d Anisotropic Permeability Simulation

For anisotropic flow Lin first transformed the geometry of the anisotropic (X,Y) system into an equivalent isotropic $(\bar{X},\bar{Y})$ system by means of the familar transformation equations:

$$\bar{X} = X/\sqrt{k_x} \; ; \; \bar{Y} = y/\sqrt{k_y} \qquad (3.13)$$

Lin's technique seemed to be a simple straightforward approach for the analysis of the complex flow geometry associated with a whole core permeameter.

CHAPTER IV

Numerical Simulation of the Whole Core Permeameter

4.1 Testing of the Finite Element Model

As in all mathematical models adequate testing must be performed to assure the validity of the methods used and the manner in which they were programmed. The testing approach for the finite element model was designed to analyze problems with known solutions. The series of problems chosen were similar to but less complex than the actual problem of interest, namely, the simulation of anisotropic flow in a whole core permeameter.

4.1a Isotropic Radial Flow

The first test was to see if the finite element model would simulate steady state isotropic radial flow described by Darcy's law in the form:

$$P_w = P_e + \frac{q_w \mu \ln(r_e/r_w)}{7.08\ kh} \qquad (4.1)$$

Recalling that ideal radial flow is axisymmetrical, only one quarter of a radial system was used for study. This not only allowed for a varification of the model's ability to simulate radial flow but also its ability to simulate isopotentials and no-flow boundaries. Figure 4-1 is a series of illustrations drawn to aid in understanding how the flow region was described. First, the ideal radial

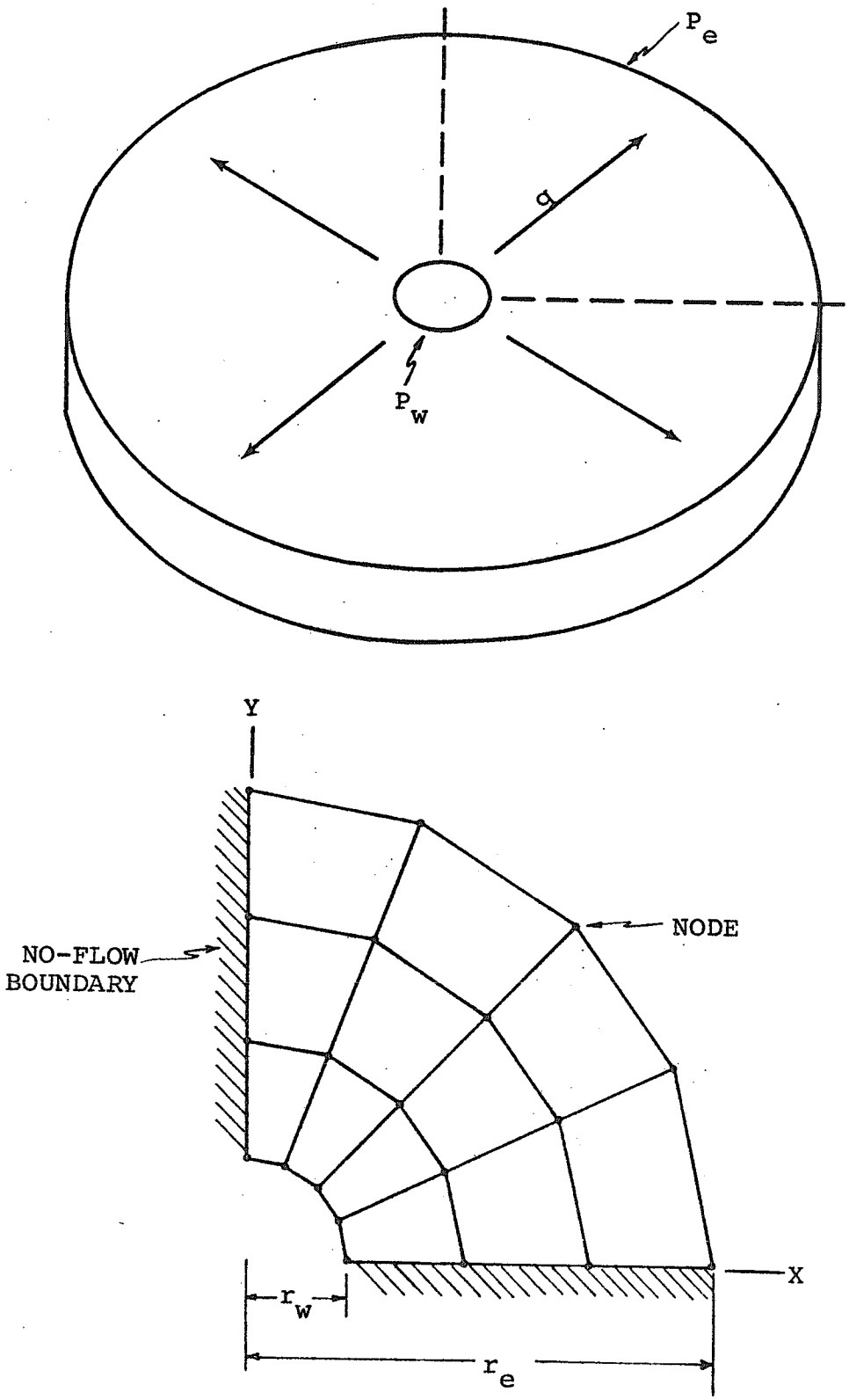

FIGURE 4-1 SCHEMATIC DRAWING OF A RADIAL FLOW SYSTEM AND THE ASSOCIATED GRID USED IN FINITE ELEMENT COMPUTATIONS.

flow region was reduced to one fourth of the total system. The resulting flow region was then divided into grids of radial character with no-flow boundaries being specified along the X and Y axes. The number of elements along the X axis was referred to as NRB, meaning the number of radial blocks while the number of elements lying on radius r_w was referred to as NCB, meaning the number of circumferential blocks. An isopotential boundary was specified at radius r_e while a uniformly distributed influx was specified over the boundary at radius r_w. The model was then run repeatedly with various internal grid densities. The prevailing potential at each node was recorded and compared with hand calculations made by use of Equation (4.1). The grid density was increased until there was no appreciable change in the results. Table 4-1 is a summary of the effects of changes in grid density. It appeared that the greater the grid density the more accurate the results. Care was taken not to use a grid density that would require an extremely large number of calculations which could ultimately result in drastic round-off errors. The results also showed that for a series of nodes located on a common radius the potentials computed by the model were equal, as to be expected in an ideal isotropic radial flow system.

4.1b Anisotropic Radial Flow

Using the apparent optimum grid density (NCB=7, NRB=35) found in the simulation of isotropic radial flow,

TABLE 4-1 EFFECTS OF VARIOUS GRID DENSITIES ON SIMULATION OF RADIAL FLOW

NCB	X	NRB	%ERROR
4	X	10	5.063
7	X	10	4.251
10	X	10	4.057
4	X	20	2.291
7	X	20	1.522
10	X	20	1.442
4	X	35	1.665
7	X	35	0.884
10	X	35	0.847

attention was then focused on an anisotropic radial system. An anisotropy ratio of 2.0 was specified in each element. The orientation of the principal axes of permeability was parallel to the X and Y axes of the grid. At radius r_w a uniformly distributed influx was specified, while at radius r_e an isopotential was specified. The model was then executed and the prevailing potential at each node recorded. Due to the uniformly distributed influx on r_w and to the anisotropic nature of the system, an isopotential on r_w was not simulated as would be required of an actual physical system. In order to realize an isopotential at r_w the influx had to be redistributed by a trial-and-error method which was both time consuming and rather tedious. After several trials an approximate radial isopotential was achieved at r_w. As would be expected for the anisotropic case the interior potential distribution along a given circular arc was not constant. Figure 4.2 is a plot of the interior potential distribution along eight particular arcs, which include the internal and external bounds of the system. Anisotropy ratios of 4.0, 6.0, 8.0, and 16.0 were investigated using the same trial-and-error technique of producing an isopotential at r_w in order to get a "feel" for the model's ability to handle anisotropic systems.

4.1c Isotropic Whole Core Permeameter

With a feeling for the model's sensitivity to anisotropy, the next step was to simulate the flow geometry in

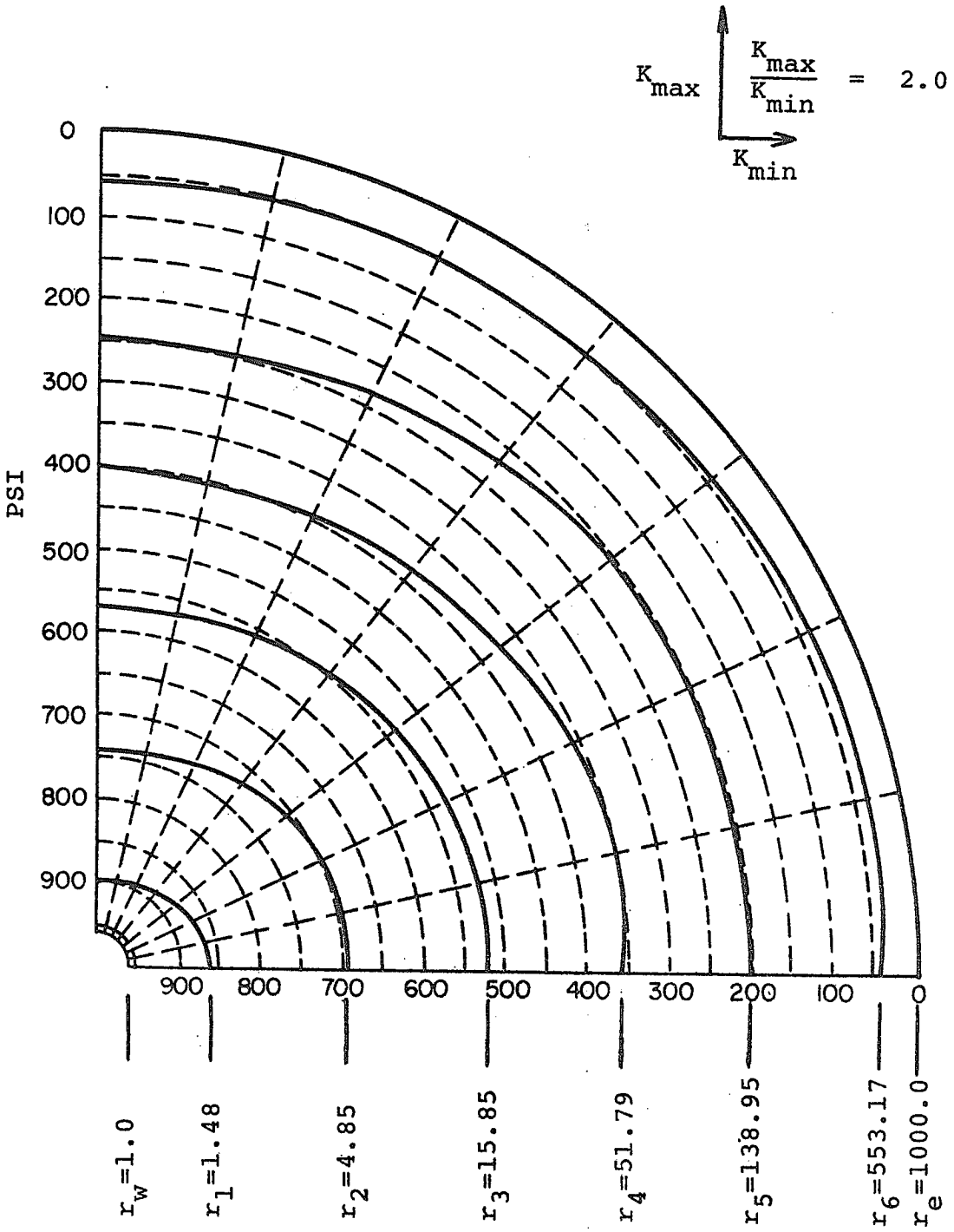

FIGURE 4-2 POTENTIAL DISTRIBUTION ALONG EIGHT DIFFERENT RADII FOR AN ANISOTROPIC RADIAL SYSTEM.

an isotropic whole core permeameter system. Since Collins' solution was available for comparison, this test seemed to be the next logical step.

Figure 4-3 demonstrates the manner in which the system was defined. Only one quarter of the parmeameter was modeled due to the symmetrical character of the isotropic flow geometry. The boundary along the X axis was specified as a no-flow boundary while the Y axis was specified as an isopotential. The circular boundary had two characteristics; the upper 80-degree portion was specified as a no-flow boundary while the lower 10-degree portion was considered to be the half-angle, α, open to flow.

The idea was to specify a certain influx over the half-angle opening and observe the resulting difference in potential across the system. Recalling that the quarter flow region would only show one half of the total drop in potential across the entire core, the observed drop would then be doubled and compared with Collins' closed form solution.

A uniformly distributed influx was specified over the angle opening and the potential at each node along the angle opening recorded. However, due to the geometry of the system the uniform influx distribution did not produce an isopotential at the influx boundary. Again a trial-and-error method of influx distribution was employed until an approximate isopotential was achieved. The potential drop

was doubled and applied to Equation (2.2) yielding a G(10°) of 1.9428. The actual value for G(10°) from Collins' curve was 2.0. The procedure was then repeated for an angle opening of 20 degrees which resulted in a G(20°) of 1.515. The actual value of a G(20°) from Collins' curve was 1.55. At this point the finite element model appeared to performing well.

Because of the time consuming and tedious task of distributing the influx over the angle opening by trial-and-error, further comparisons with the closed form solution would have been a very laborious task unless some numerical method of influx distribution could be developed.

4.1d Influx Distribution by Superposition

From previous experiences with the effects of different influx distributions, the principle of superposition appeared to be a straightforward approach to the problem. Figure 4-4 demonstrates the procedure used. The model was executed specifying a unit influx, q_1, across the side of only one element on the angle opening, while the influx across the remaining element sides was set at zero, (Step 1). At each of the several nodes on the angle opening, the potential resulting from the single influx q_1 was recorded. In a similar manner, this procedure was repeated for Steps 2 through 4. In each succeeding step, the single unit influx was introduced across a different segment of the inflow boundary and the potential at all nodes on this boundary

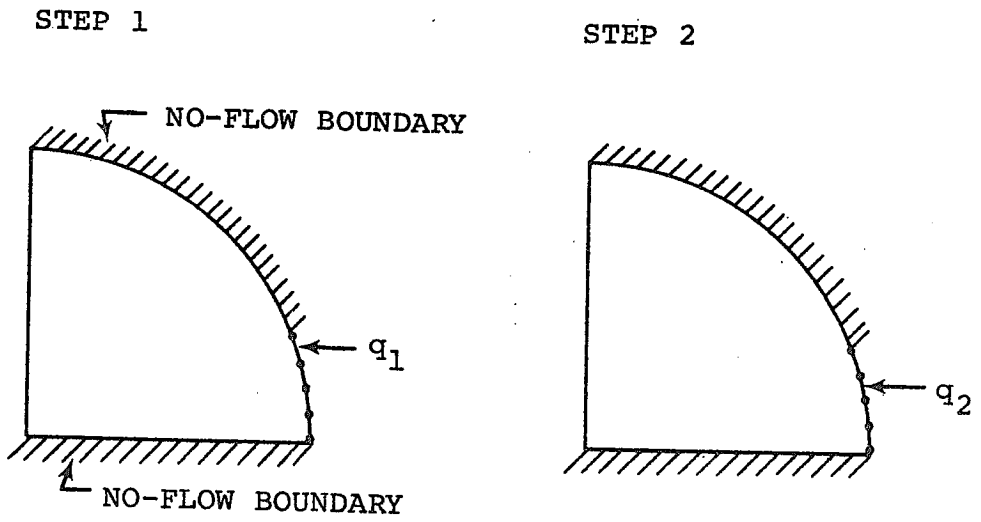

$$q_1 = q_2 = q_3 = q_4 = 1.0$$

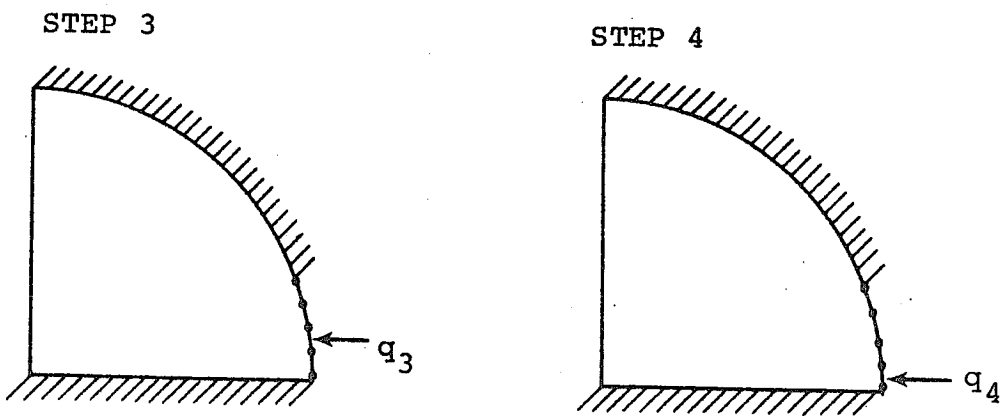

FIGURE 4-4 INITIAL STEPS USED IN THE SUPERPOSITION PROCEDURE OF INFLUX DISTRIBUTION FOR THE ISOTROPIC WHOLE CORE SYSTEM.

was recorded.

For the case where a unit influx is introduced simultaneously across each segment of the inflow boundary, the resulting potential at any node on the boundary would then be given by

$$P_j = \sum_{i=1}^{W} p_{j,i} \tag{4.2}$$

where $p_{j,i}$ is the potential computed for node j in Step i, i.e., with a unit influx across segment i of the boundary and no influx across the remainder of the boundary. The total number of segments which span the inflow boundary is denoted by W.

A more practical consideration is the case where the total influx into the system is specified as q_1, q_2,....., q_w, where the individual influx rates, q_i, are not all unity. As a consequence of Darcy's law, the resulting potential, P_j at each node along the inflow boundary would be given by

$$P_j = \sum_{i=1}^{W} p_{j,i}\, q_i; \quad [j=1,2,...W, (W+1)] \tag{4.3a}$$

In matrix notation, this series of linear equations may be written as

$$\begin{bmatrix} p_{1,1} & p_{1,2} \cdots p_{1,w} \\ p_{2,1} & p_{2,2} \cdots p_{2,w} \\ \vdots & \vdots \\ p_{w+1,1} \cdots\cdots & p_{w+1,w} \end{bmatrix} \begin{bmatrix} q_1 \\ q_2 \\ \vdots \\ q_w \end{bmatrix} = \begin{bmatrix} P_1 \\ P_2 \\ \\ P_{w+1} \end{bmatrix} \qquad (4.3b)$$

or, in a more compact form as

$$AQ = P \qquad (4.3c)$$

We see that A is a (W+1) by (W) matrix while Q is a column vector of order W and P a column vector of order W+1. To test the validity of the superposition technique, an arbitrary influx distribution was specified for the permeameter. The computed potentials at all nodes along the inflow boundary were then recorded. Next, this same influx distribution was used as the elements of the Q vector in Equation (4.3b). The resulting potentials as computed by superposition were then compared to those previously recorded and were found to be identical. This same test procedure was repeated for numerous influx distributions and the results were always favorable.

With the superposition technique firmly established, Equation (4.3b) suggested that a converse problem should also be amenable to solution. That is, for a given isopotential vector, P, it should be possible to solve for the associated influx vector, Q. This would allow one to specify an isopotential along the inflow face and then solve for the associated influx distribution-avoiding the

previous trial-and-error solution of this problem.

Due to the non-square nature of the A matrix, three different solution techniques were attempted in an effort to solve the Q vector associated with a given P vector. The first technique was based on the assumption that the error introduced by dropping one of the (W+1) equations could be tolerated. This would reduce the A matrix to a square which could then be solved by Gauss elimination. A series of runs was made to determine which of the equations, if any, could be dropped with the least amount of error. Each of the rows in Equations (4.3b) was dropped, one at a time, and the Q vector was found using Gauss elimination. However, the resulting solutions were obviously in error since they admitted efflux from the core across certain segments along the inflow boundary and influx across some others. Round-off error was thought to be one source of trouble, so the entire model was changed to double precision, including the generation of the A matrix. However, the results obtained from the double precision model were no better than before. The same set of equations were solved by means of an iterative procedure taken from IBM's Scientific Subroutine Package called "RSLMC." Again there was no improvement in the results, thus ruling out the possibility of round-off error in the previous Gauss elimination procedure.

The second approach tried involved adding any two of the equations in order to again reduce the A matrix to a square. However, the resulting Q vector contained some negative elements which again admitted efflux across certain segments of the inflow boundary.

Finally, a third method with a more sound mathematical bases was tried. This method of solving a non-square matrix equation involved the application of the following theorem:

$$A^T A Q = A^T P \qquad (4.4)$$

where A^T is the transpose of A. As the product of A^T A is a square matrix, this again reduces the problem to solving (W) equations in (W) unknowns. The influx vector, Q, was obtained by Gauss elimination. Even though the entire procedure was carried out in double precision the results again were unreasonable.

At this point the following possible sources of error were investigated:

1. Perhaps the original A matrix generated by the finite element model was not correct.
2. Perhaps the choice of the shape and size of the elements along an inflow boundary have some hidden restrictions.
3. Perhaps an influx could only be specified over one side of an element.

The evaluation of the first possible source of error mentioned above was accomplished by again considering the radial flow system for which the solution was known. The test employed the superposition procedure developed for the whole core geometry and can best be understood by considering Figure 4.5. A common injection rate, q_i, was specified over one element side on r_w at a time, thus generating an A matrix applicable to this radial flow geometry. The total potential at each node on r_w was then calculated for a specified Q vector by Equation (4.3b). These potentials were then compared with those obtained by the use of the original finite element model. The results were identical. This confirmed the fact that the method for generating the A matrix was valid for the radial geometry and hence for the whole core geometry. The converse problem was also tested in this radial system, i.e., for a given isopotential P vector the correct Q vector was obtained.

The next test was conducted to study the effects of the shape of the elements along the inflow boundaries. Recalling that the model was designed to work with quadrilateral elements without restricting their size or shape, consider the grid of the whole core flow region shown in Figure 4-3. It should be noted that the elements on the inflow boundary were of a triangular nature. It should also be noted that the finite element model subdivides each

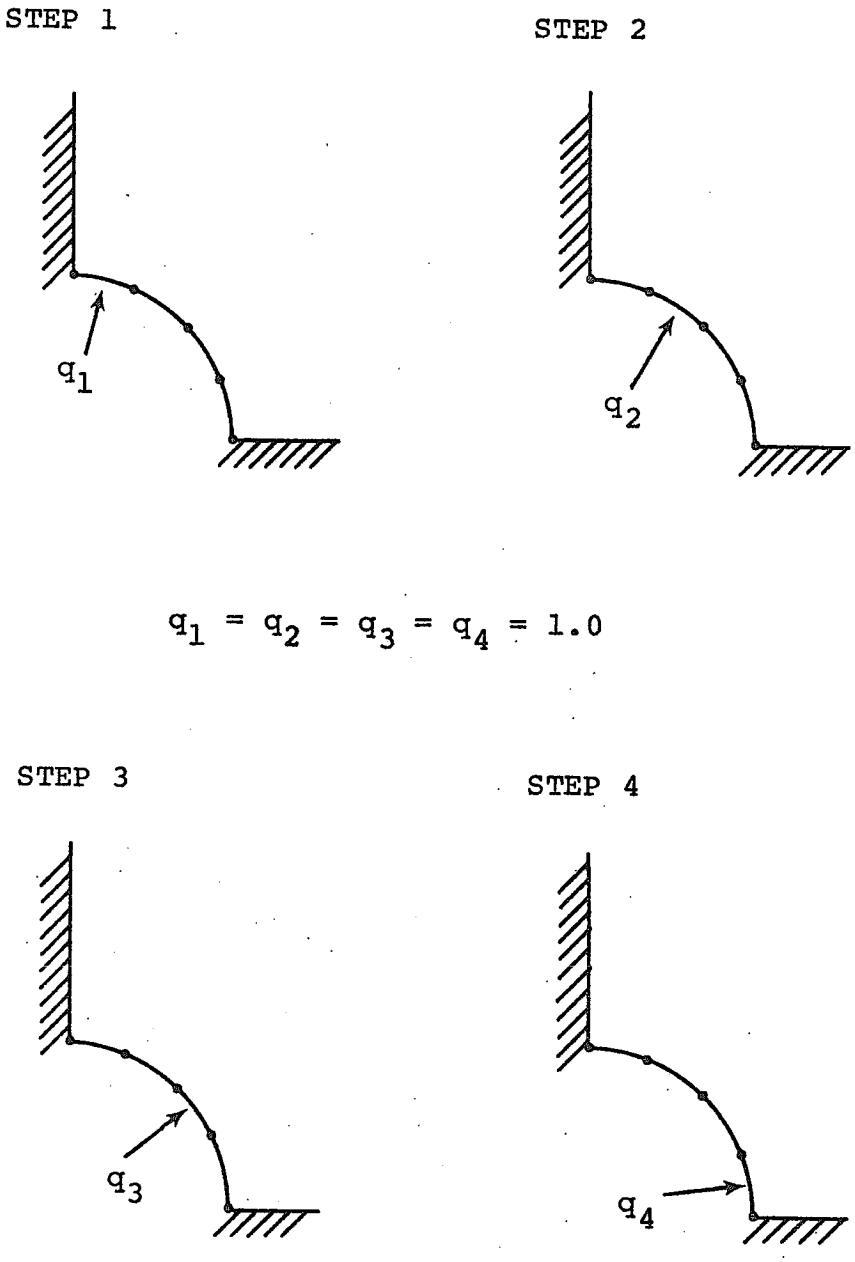

FIGURE 4-5 INITIAL STEPS USED IN THE SUPERPOSITION PROCEDURE OF INFLUX DISTRIBUTION FOR THE ISOTROPIC RADIAL SYSTEM.

of the quadrilateral grid elements specified in the program input into four included triangles before the potential functions are applied. The subdivision of a square or a rectangular element should be accomplished without fear of round-off error affecting the final definition of co-ordinates of the resulting four triangles. This same argument is not convincing for the case of the boundary quadrilateral elements of Figure 4-3 which are essentially triangular at the outset. The testing of the idea that round-off error was affecting the definition of the triangular sub-elements, thus causing the erroneous results, was accomplished by again referring back to the radial flow system. A new grid of the radial flow region was devised that contained quadrilateral elements of a triangular nature along the inflow boundary, r_w (see Figure 4-6). When this grid was applied to the model the results were very representative of those for ideal radial flow. Several grids were tried in an effort to increase the chance of round-off error by reducing the length of the shortest side of the elements. The results were still very representative of radial flow.

Finally a grid was designed to expose two sides of each quadrilateral element along the area open to flow (see Figure 4-7). This was to test the model's ability to handle a specified flow across two sides of a boundary element. A uniformly distributed influx was specified

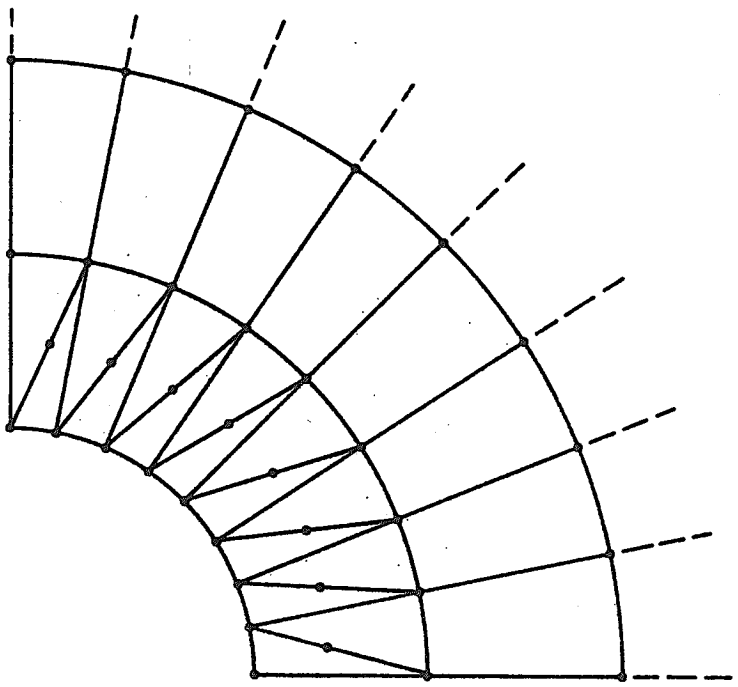

FIGURE 4-6 GRID FOR TESTING TRIANGULAR ELEMENTS ON THE INFLOW BOUNDARY OF A RADIAL SYSTEM.

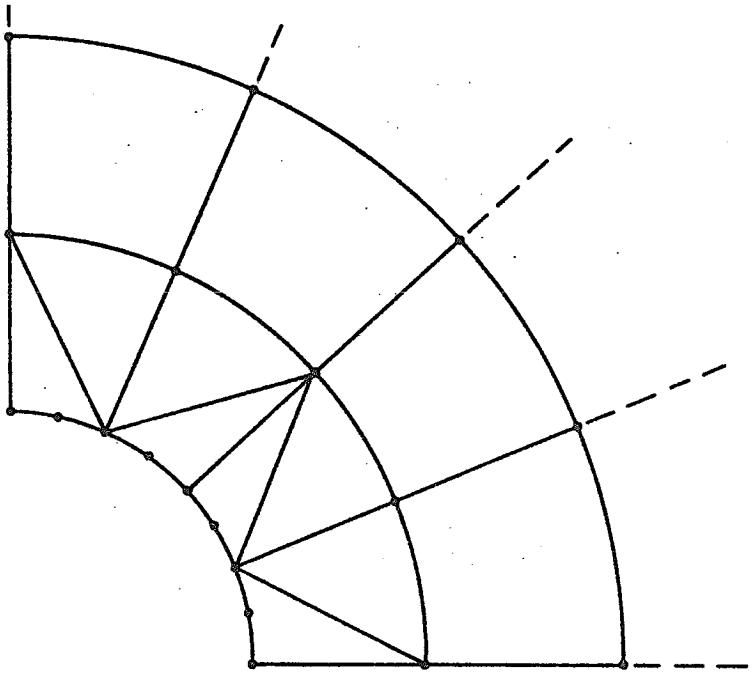

FIGURE 4-7 GRID FOR TESTING BOUNDARY ELEMENTS HAVING INFLUX SPECIFIED OVER TWO SIDES.

over r_w. The superposition technique was applied which not only produced radial isopotentials indicative of radial flow but also reproduced the same uniform influx distribution when the Q vector was solved. These results not only verified the model's ability to handle specified flow across two sides of an element but again pointed out the validity of the superposition method of influx distribution. Having extensively tested the validity of the superposition method of influx distribution and finding no apparent reason why the results computed for the isotropic whole core geometry were unreasonable-aside from the complexity of this flow geometry-another type of mathematical model was considered.

4.2 Image Wells and Streamline Model

As discussed in Chapter III the technique of image wells and streamline tracking appeared to be a rather straight-forward approach for simulating the complex flow geometry of the whole core permeameter. This technique involved generating and solving a series of linear equations which stem from Equation (3.7). However, several different forms of these linear equations were considered due to the various ways in which the boundary conditions were treated. As seen in Figure 3-1 there are isopotential boundaries, no-flow boundaries, and areas of discontinuity to be simulated before a valid study of anisotropic permeability can be made. The remainder of

this chapter is devoted to the different techniques used to simulate these boundary conditions for the case of an isotropic system where K_x and K_y equal 1.0 and where the half-angle opening, α, equals 20 degrees.

4.2a All Image Well System

An all image well system means that all of the boundary well strengths were calculated, i.e., there were no specified well strengths.

Consider the system shown in Figure 4-8. The 18 image wells were spaced 20 degrees apart and 500-ft from the circular boundary of 2000-ft diameter. There were 30 no-flow boundary pairs of points describing the no-flow boundaries B and B'. The isopotential boundaries A and A' were described by assigning a common potential to the 5 points on each boundary such that the potential on boundary A was greater than the potential on boundary A'. This was to assure flow from A to A'. When applying Equation (3.7) the following set of linear equations was generated:

For the no-flow boundary

$$\sum_{j=1}^{N} q_j \ln\left[\frac{K_y(XI_i-XW_j)^2 + K_x(YI_i-YW_j)^2}{K_y(XS_i-XW_j)^2 + K_x(YS_i-YW_j)^2}\right] = 0.0 \qquad (4.5a)$$

For the isopotential boundaries, A and A'

$$\sum_{j=1}^{N} q_j \ln\left[\frac{(XPL_k-XW_j)^2}{K_x} + \frac{(YPL_k-YW_j)^2}{K_y}\right] = \frac{(C-PL_k)4\pi h\sqrt{K_xK_y}}{\mu} \qquad (4.5b)$$

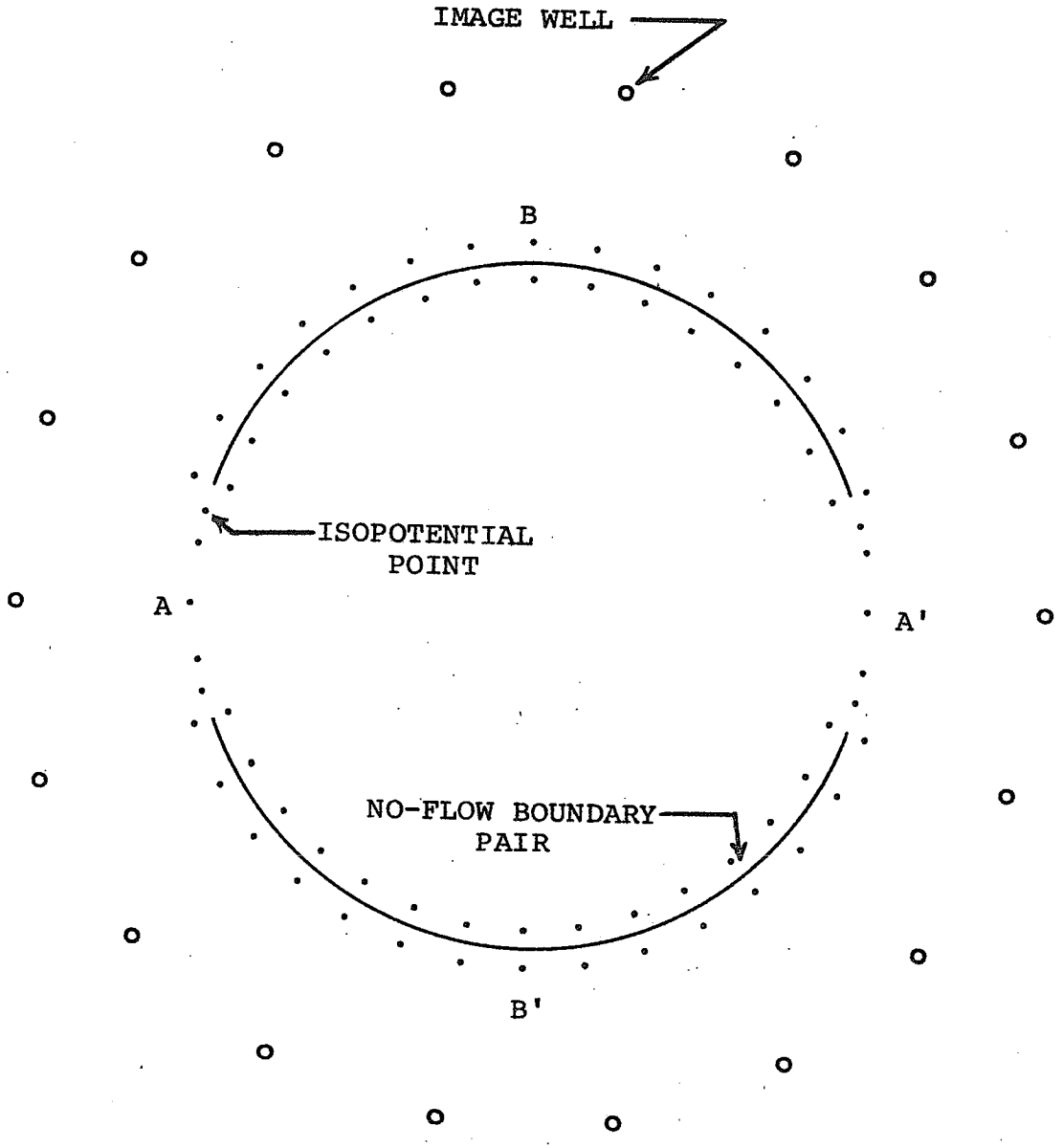

FIGURE 4-8 BASIC PATTERN OF IMAGE WELLS AND CONTROL POINTS USED TO SIMULATE THE ISOTROPIC FLOW GEOMETRY OF THE WHOLE CORE PERMEAMETER.

$$\sum_{j=1}^{N} q_j \ln\left[\frac{(XPR_k - XW_j)^2}{K_x} + \frac{(YPR_k - YW_j)^2}{K_y}\right] = \frac{(C - PR_k)\, 4\pi h \sqrt{K_x K_y}}{\mu} \qquad (4.5c)$$

where:

XI_i, YI_i = co-ordinates of one exterior point of a no-flow boundary pair.

XS_i, YS_i = co-ordinates of one interior point of a no-flow boundary pair.

XW_j, YW_j = location of an image well.

XPL_k, YPL_k = co-ordinates of a point on the left isopotential, A.

XPR_k, YPR_k = co-ordinates of a point on the right isopotential, A'.

PL_k and PR_k = specified potential on A and A', respectively.

N = number of image wells.

It should be noted that for this system the only unknowns were the strengths of the image wells, q_j's, which are elements of a yet undefined Q vector. Also, there were more no-flow boundary pairs than image wells which yielded more equations that unknowns. Hence, a set of linear equations comparable to those in Equation (4.3b) was realized. The solution to these equations was carried out by applying Equation (4.4) and then solving for the Q vector by Gauss elimination. Once the individual q_j values were found, several of the streamlines within the

flow region were traced (see Figure 4-9). The results show that isopotentials along A and A' were not realized. This was evident since the streamlines were not perpendicular to A and A', and the calculated potentials on A and A' were not constant. These potentials were obtained from Equation (3.7) and the elements of the Q vector. Also, the symmetry of this isotropic system was not simulated as can be seen upon comparison of the strengths of the image wells.

In the previous attempt to simulate the flow geometry recall that only 5 points on each isopotential were specified. These 10 points provided 10 of the equations involved in the solution for the Q vector, which in turn influenced the calculated potentials on A and A'. The second simulation attempt was made by specifying 19 points on each isopotential in hopes that the influence of a large number of equations would result in a better simulation of the isopotentials. However, the results did not show any improvement.

The next attempt was to increase the definition of the angle open to flow. More image wells were placed adjacent to these areas. The calculated potentials on A were nearly the same, but the potentials on A' did not approximate an isopotential. The no-flow boundaries also leaked, the streamlines were not perpendicular to A and A', nor were the strengths of the image wells symmetrical.

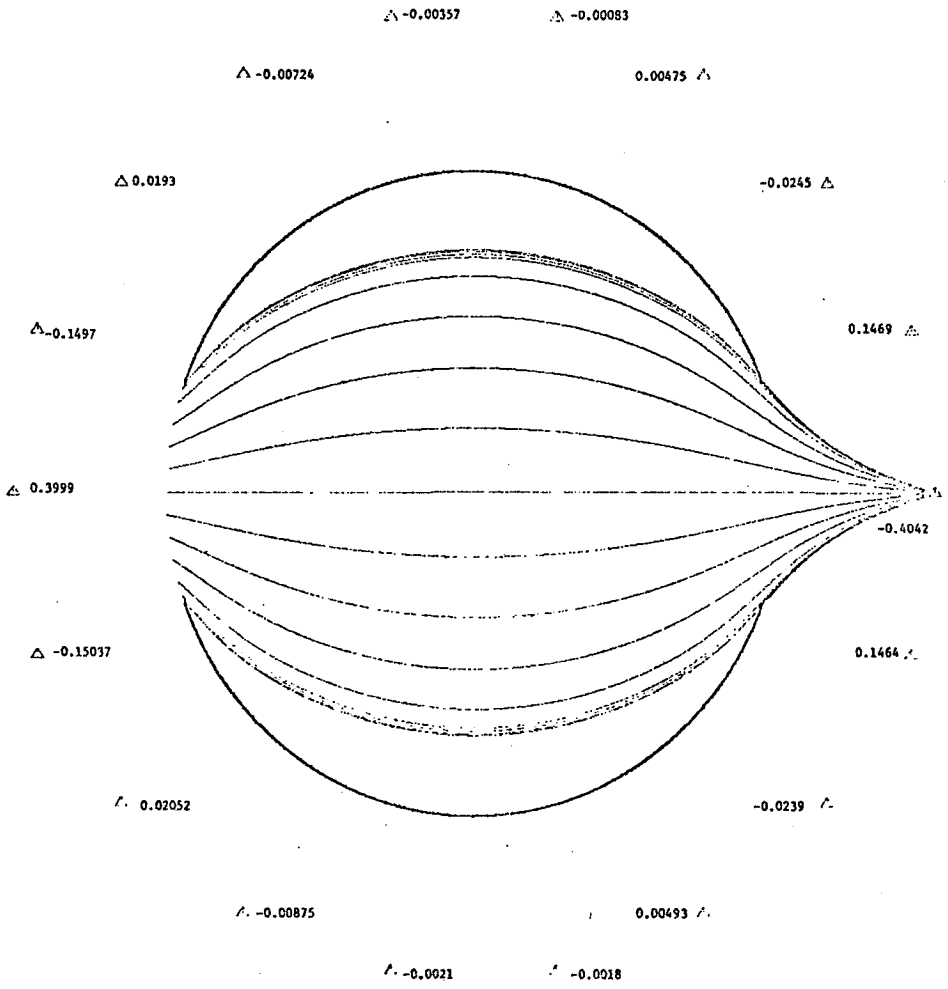

FIGURE 4-9 COMPUTED WELL STRENGTHS AND STREAMLINES FOR A SYSTEM OF 18 IMAGE WELLS, 30 NO-FLOW BOUNDARY PAIRS AND 5 POINTS ON AN ISOPOTENTIAL.

In an effort to better bound the flow region a second row of image wells were placed exterior to the original row of wells (see Figure 4-10). The results of this simulation showed that the no-flow boundaries appeared to be well defined. However, the simulation of the A' isopotential again was a failure, and the streamlines still did not behave properly.

4.2b System Wells and Image Wells

Having attempted to simulate the flow geometry using an all image well system without success, a different approach was tried. In this approach some of the image wells were given specific strengths. It was felt that more control over the areas open to flow could be had by the use of these system wells. The idea was to create the isopotentials by a clever choice of locations and strengths for the system wells. For added control the points on the isopotential boundaries were paired as were those for the no-flow boundaries. The only difference was that these isopotential pairs fell on a boundary instead of on opposite sides of a boundary. Different pairing schemes were also tried as will be seen in the examples.

These changes resulted in the generation of a different series of linear equations. For example, consider Figure 4-11. The resulting set of linear equations are of the form:

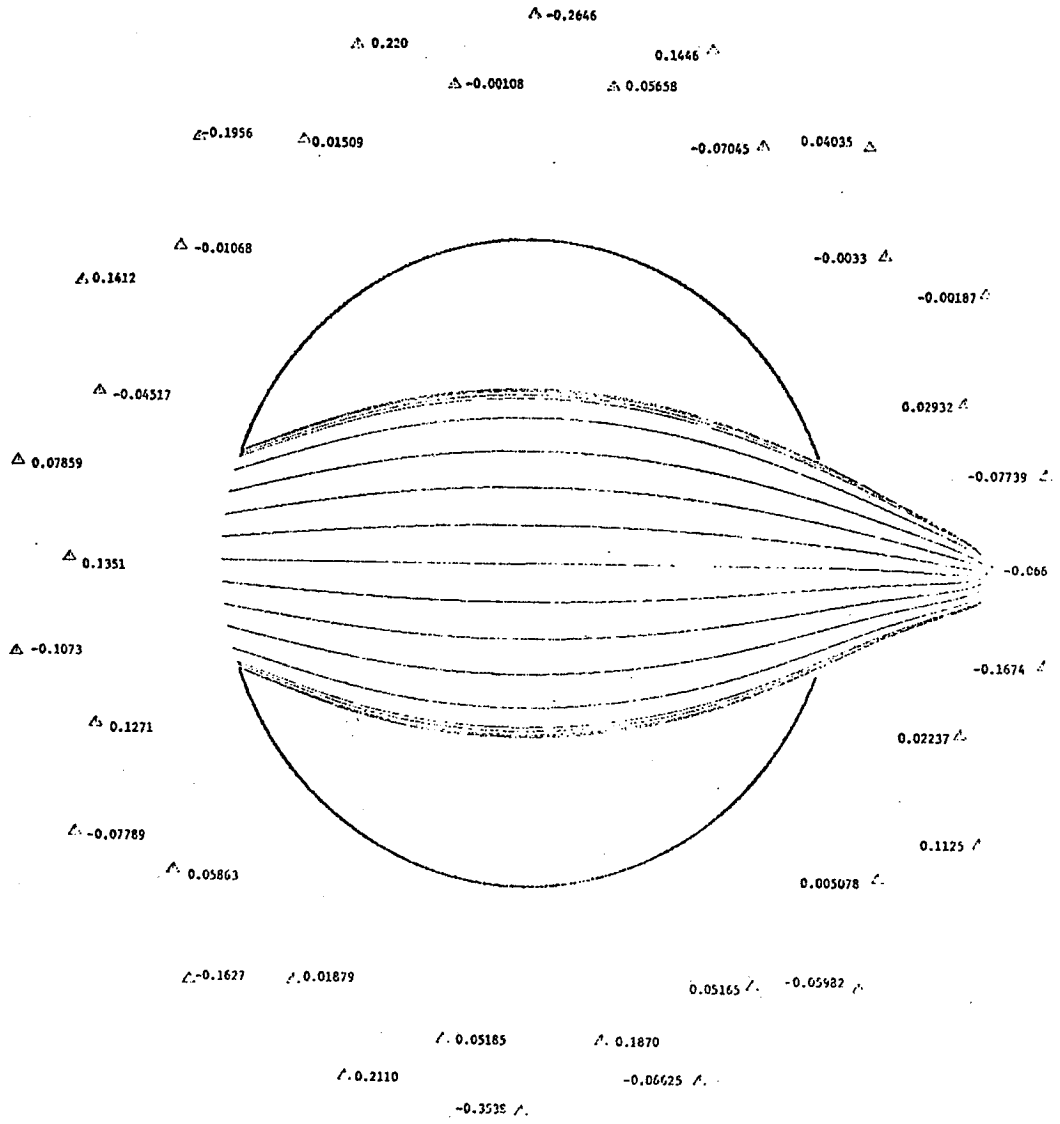

FIGURE 4-10 COMPUTED WELL STRENGTHS AND STREAMLINES FOR A SYSTEM OF 36 IMAGE WELLS.

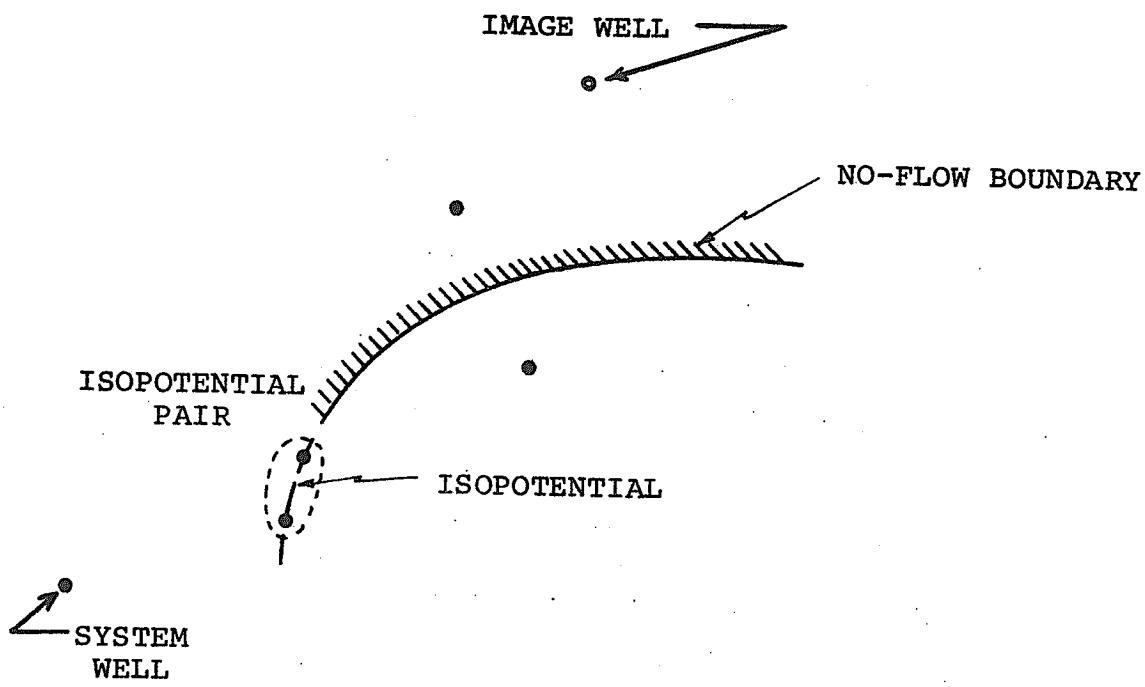

FIGURE 4-11 SCHEMATIC DRAWING SHOWING PAIRS OF POINTS USED TO DESCRIBE EITHER ISOPOTENTIAL OR NO-FLOW BOUNDARIES, A REPRESENTATIVE SYSTEM WELL AND AN IMAGE WELL.

$$\sum_{j=1}^{N} q_j \ln\left[\frac{K_y(XS_i-XW_j)^2 + K_x(YS_i-YW_j)^2}{K_y(XI_i-XW_j)^2 + K_x(YI_i-YW_j)^2}\right] =$$

$$\sum_{m=1}^{NS} q_m \ln\left[\frac{K_y(XI_i-XSW_m)^2 + K_x(YI_i-YSW_m)^2}{K_y(XS_i-XSW_m)^2 + K_x(YS_i-YSW_m)^2}\right] \qquad (4.6)$$

where:

q_m = the strength of a system well.

XSW_m, YSW_m = the location of a system well.

N = the number of image wells.

NS = the number of system wells.

The only unknowns are the q_j values for the image well strengths which are the elments of the Q vector. The solution to the Q vector was the same as in section 4.2a.

The first attempt to simulate the whole core flow geometry was defined in the following manner:

1. There were 30 no-flow boundary pairs as in all of the previous examples.
2. There were a total of 80 isopotential pairs - 40 on each isopotential boundary. Each point was paired with the adjacent point.
3. There were 10 system wells - 5 injectors equal to 100.0 and 5 producers equal to - 100.0 (see Figure 4-12).
4. There were 12 image wells.

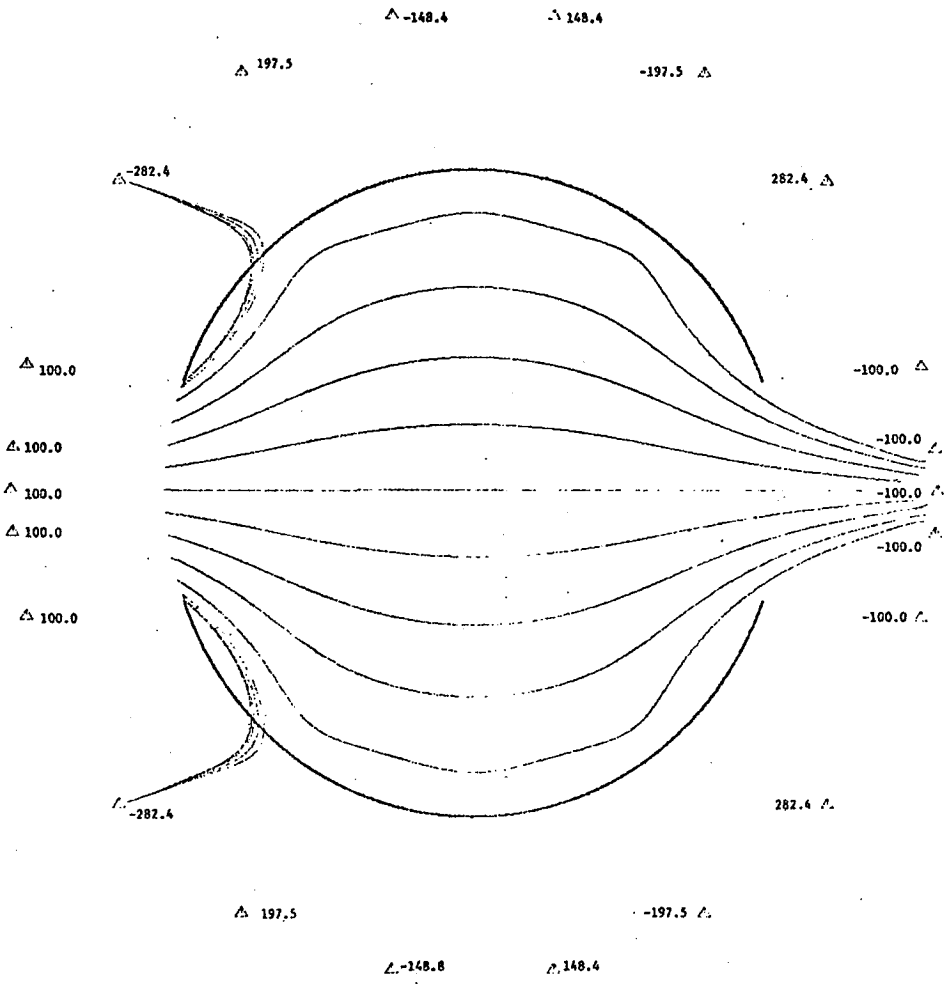

FIGURE 4-12 COMPUTED STREAMLINES AND IMAGE WELL STRENGTHS FOR A SYSTEM OF 12 IMAGE WELLS AND 10 SYSTEM WELLS.

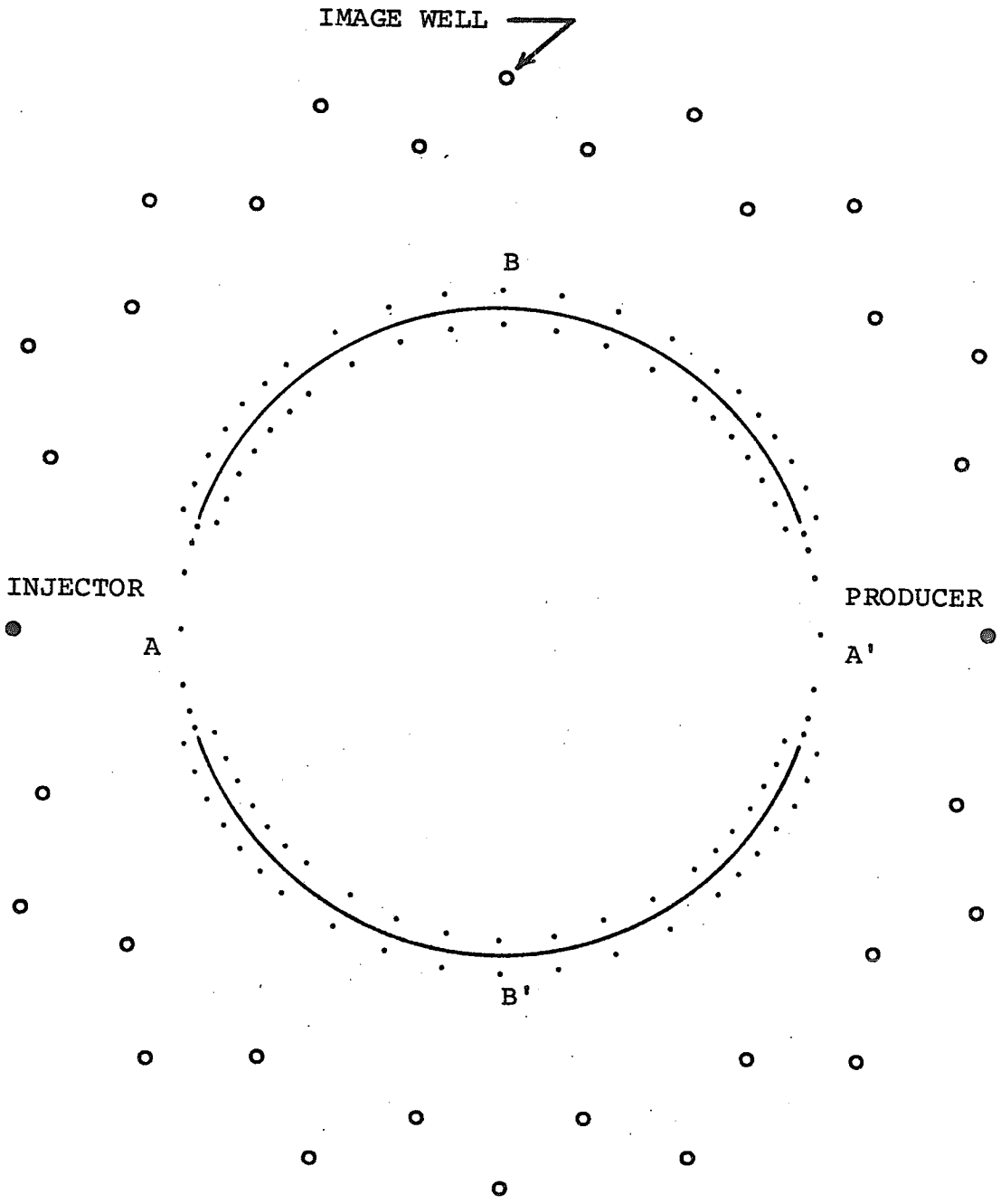

FIGURE 4-13 STAGGERED IMAGE WELL PATTERN AND ADDITIONAL NO-FLOW BOUNDARY PAIRS USED TO REDUCE LEAKAGE ACROSS THE NO-FLOW BOUNDARIES.

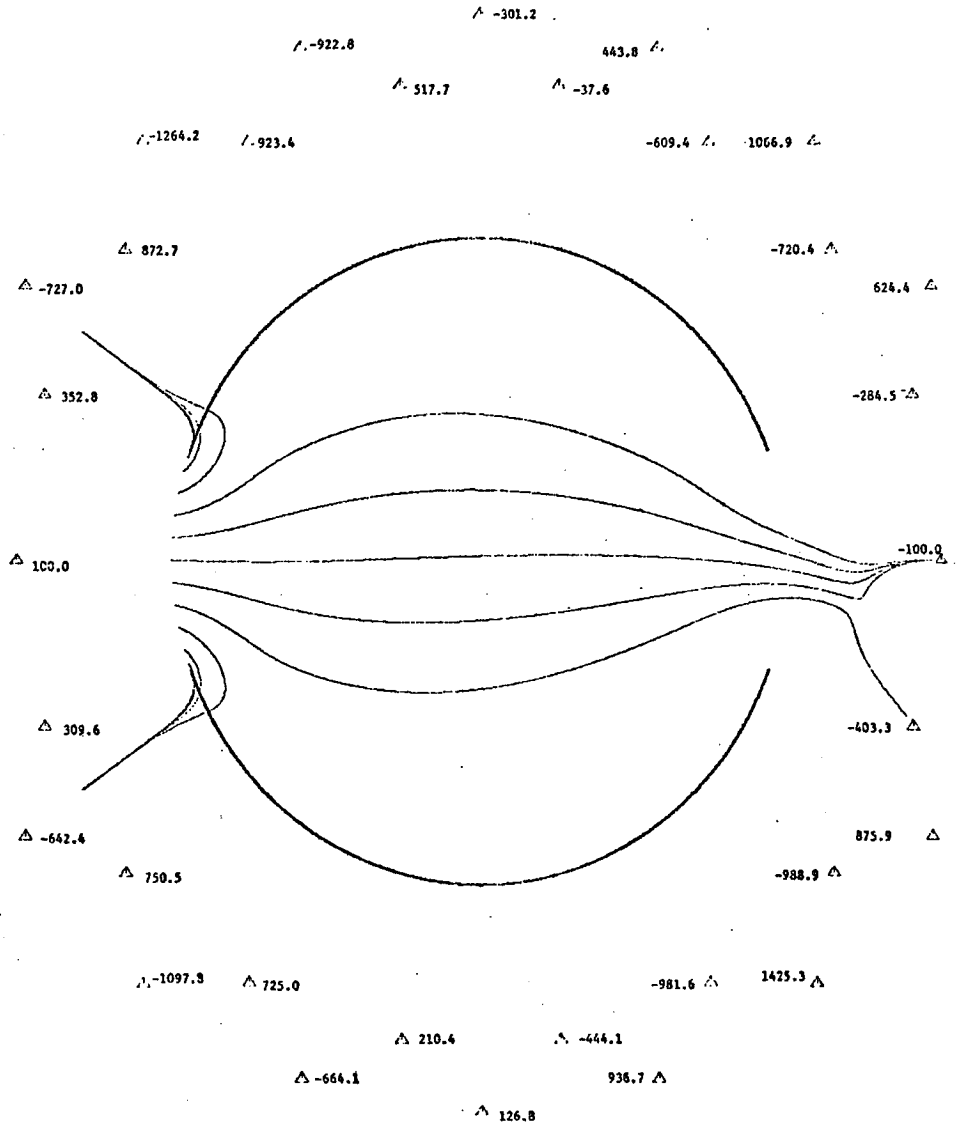

FIGURE 4-14 REDUCTION OF LEAKAGE BY USE OF 2 SYSTEM WELLS, A STAGGERED IMAGE WELL PATTERN AND ADDITIONAL NO-FLOW BOUNDARY PAIRS.

4.2c Improved Definition Near Discontinuities

In most reservoir models areas of discontinuity must be given careful consideration in order that their influence is not overly propagated throughout the system of interest. Such influence could lead to erroneous results.

With this in mind more detail was specified in the areas of discontinuity of the whole core geometry (see Figure 4-15). Not only were there more no-flow boundary pairs near the no-flow and isopotential boundaries but these pairs were tapered in an effort to allow the maximum flow around these corners without leakage across the no-flow boundary. Also, the well locations around these areas where changed to help control the flow of fluid. Various combinations of system wells and image wells were tried with the most promising being that of Figure 4-16, where there are 5 producers and 5 injectors specified. The areas of discontinuity appeared to be free from leakage as can be seen by the streamline behavior in these vicinities. The image wells appear to be nearly symmetrical in strength. However, the isopotentials still were not simulated satisfactorily in that the streamlines did not cross at right angles nor were the calculated potentials representative of an isopotential boundary.

Recalling that Muskat[13] has shown that for an infinite array of wells, i.e., a line drive, isopotentials parallel to the line of wells develop at a distance from the line

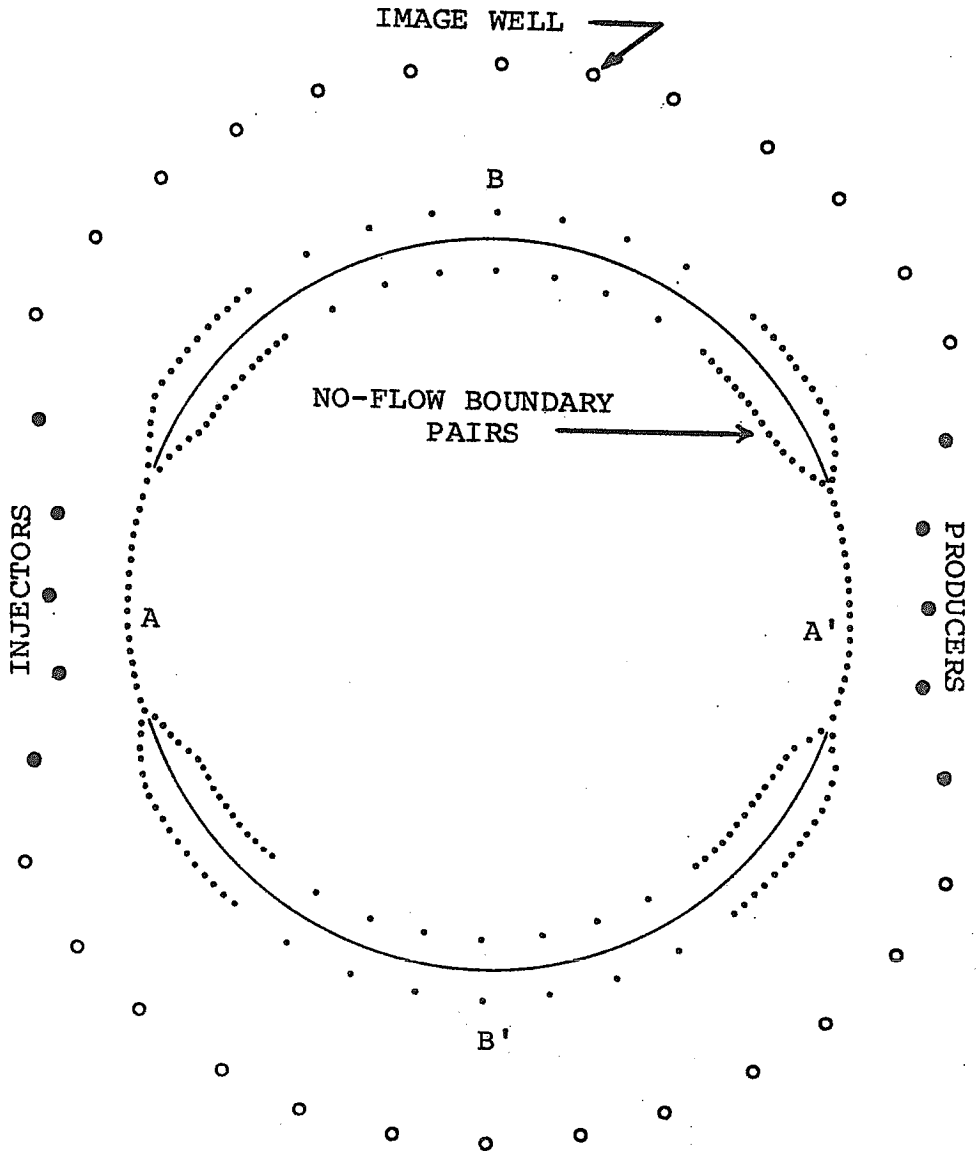

FIGURE 4-15 PATTERN OF NO-FLOW BOUNDARY PAIRS USED TO ELIMINATE LEAKAGE ACROSS THE NO-FLOW BOUNDARIES.

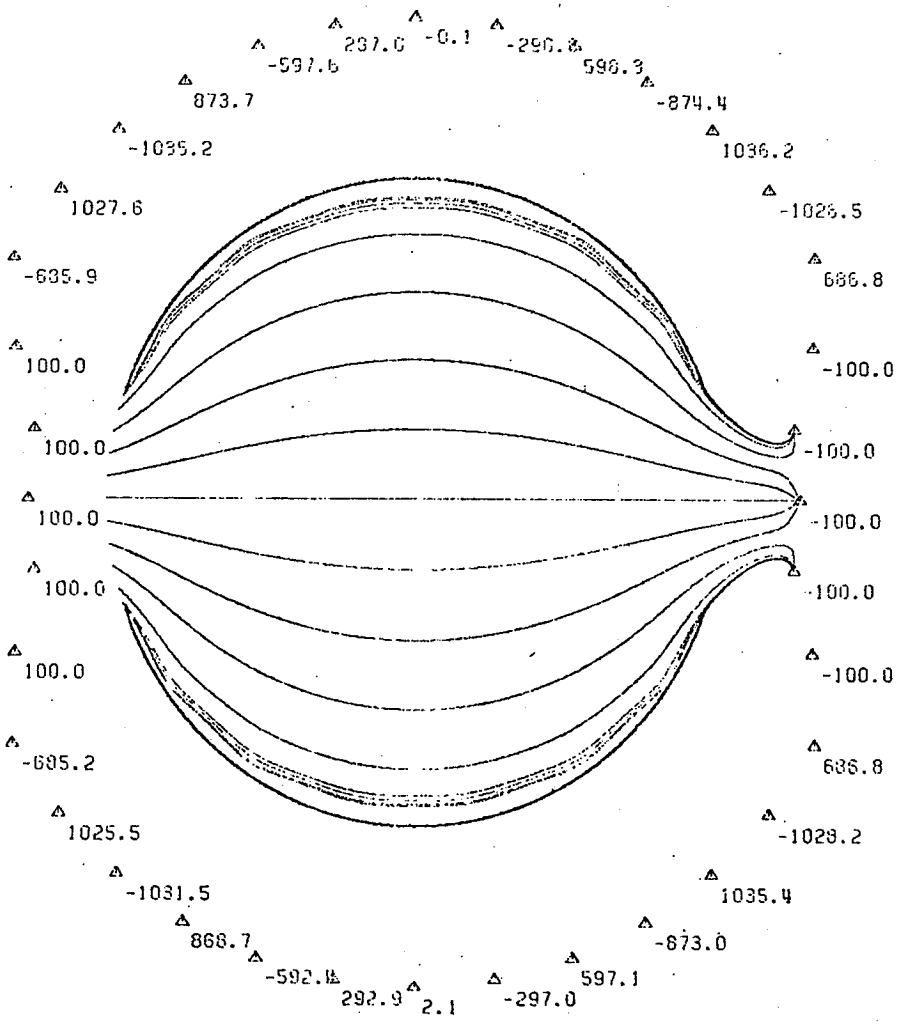

FIGURE 4-16 IMPROVED FLOW GEOMETRY WITH SYMMETRICAL IMAGE WELL STRENGTHS AND NO APPARENT LEAKAGE.

source equal to the common well spacing. With this fact in mind and recalling that the desired isopotential is more of an arc than a straight line, the positions of the system wells were changed to approximate the arc-shaped isopotential. Additional wells were introduced to help approximate a line source. The results showed promise since the angles at which the streamlines crossed the isopotential boundaries were affected by the number of system wells and their distance from the isopotential boundaries. However, the calculated potentials were not representative of an isopotential, nor did the streamlines cross at right angles (see Figure 4-17).

4.2d Attempt to Improve Streamline Control

Finally, an added restriction was imposed on the system in an effort to force the streamlines to cross the isopotentials at right angles. Recall that for two lines to be perpendicular there slopes must be negative reciprocals of each other. With the equation of the line on which the isopotential falls represented as

$$r^2 = y^2 + x^2 \tag{4.7a}$$

and the slope of the streamlines represented as

$$\frac{V_y}{V_x} = \text{slope of streamline} \tag{4.7b}$$

the following series of linear equations were added to the

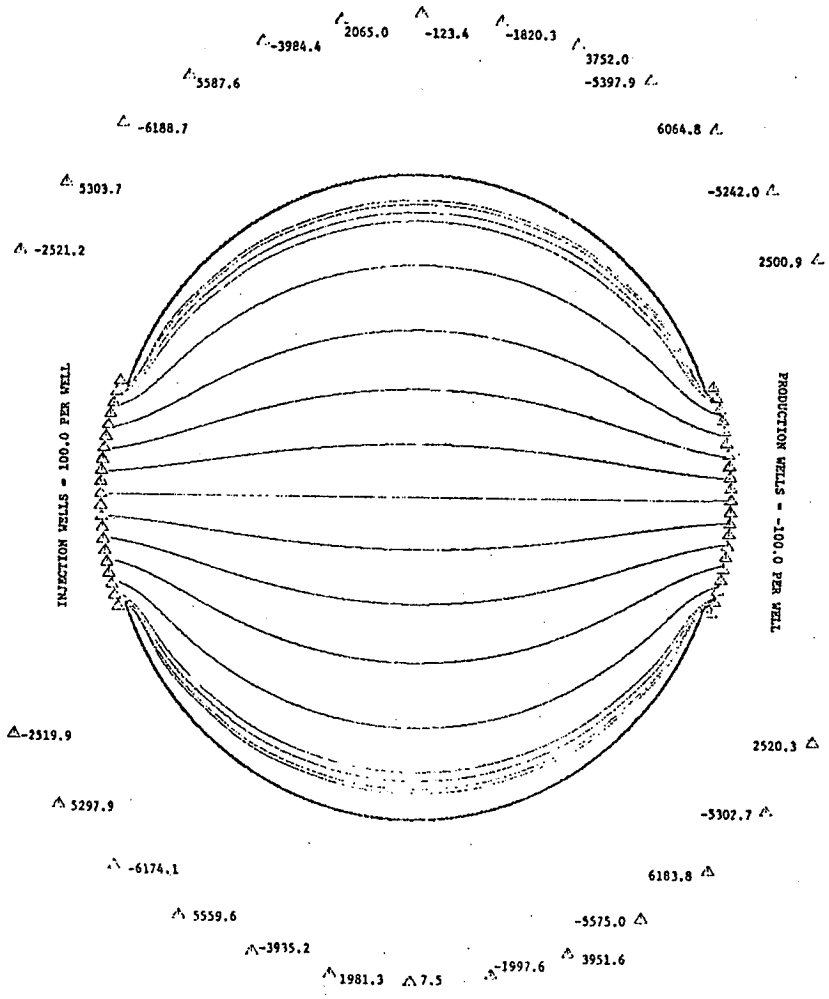

FIGURE 4-17 RESULTS OBTAINED USING 21 SYSTEM WELLS LOCATED ON AN ARC ADJACENT TO A DESIRED ISOPOTENTIAL.

case of an "All image well system:"

For YPL_k or $YPR_k \geq 0$

$$\sum_{j=1}^{N} q_j \left[\frac{(Y-YW_j) - (X-XW_j)(r^2-x^2)^{1/2}}{K_y(X-XW_j)^2 + K_x(Y-YW_j)^2}\right] = 0.0 \qquad (4.8a)$$

For YPL_k or $YPR_k \leq 0$

$$\sum_{j=1}^{N} q_j \left[\frac{(Y-YW_j) + (X-XW_j)(r^2-x^2)^{1/2}}{K_y(X-XW_j)^2 + K_x(Y-YW_j)^2}\right] = 0.0 \qquad (4.8b)$$

The results from this added restriction yielded a fairly well defined isopotential on boundary A but not on A'. Also, the resulting streamlines were not perpendicular to the isopotential boundaries.

While the image well and streamline model has yet to perform satisfactorily it is felt that additional modifications in handling the boundary conditions might improve its performance.

CHAPTER V

Conclusions and Recommendations

5.1 Conclusions

This study of simulating the flow geometry of a whole core permeameter yielded the following conclusions:

1. The simulation of anisotropic whole core permeameter flow geometry appears to be feasible by means of a finite element approach, however it involves a rather tedious and time consuming trial-and-error process of influx distribution.
2. To eliminate the trial-and-error influx distribution process of the finite element approach, the method of superposition does not appear to be reasonable.
3. In its present form the image well and streamline model will not satisfactorily simulate isopotentials on the boundaries open to flow.
4. The simulation of no-flow boundaries for this particular geometry appears to be feasible with the image well and streamline model by use of a series of tapered no-flow boundary pairs.

5.2 Recommendations

1. It is recommended that a better technique of influx distribution be developed for the finite element approach. Also, more investigations

should be made with the trial-and-error technique of influx distribution to study different anisotropy ratios and angle openings.

2. It is recommended that a study be made of the number of wells and their locations around the areas of discontinuity for the image well and streamline model in order to improve the simulation of isopotential boundaries.

BIBLIOGRAPHY

1. Barfield, E. C., Jordan, J. K., and Moore, W. D.: "An Analysis of Large Scale Flooding in the Fractured Spraberry Trend Area Reservoir," J. Pet. Tech. (April, 1959) 15.

2. Collins, R. E.: Flow of Fluids Through Porous Materials, Reinhold Publishing Corp., New York, N. Y. (1961), 93-98.

3. Cooley, R. and Peters, J.: "Finite Element Solution of Steady State Potential Flow Problems," U.S. Army Corps of Engineers, Sacramento, CA. (November, 1970).

4. Fettke, C. R.: "The Bradford Oil Field, Pennsylvania and New York," Penna. Geol. Survey, Fourth Series, Bull. M21 (1938), 203.

5. Greenkorn, R. A., Johnson, C. R., and Slallenberger, L. K.: "Directional Permeability of Heterogeneous Anisotropic Porous Media," TRANS, AIME (1964) 231. 124-132.

6. Holden, W. R.: "Permeability Microstratification in Natural Sandstones," Ph.D. Dissertation, The University of Texas (January, 1969).

7. Hutchinson, C. A., Jr.: "A Frontier in Reservoir Technology: Reservoir Inhomogeneity Assessment and Control," The Pet. Engr. (September, 1959) 31, No. 10, B-19.

8. Johnson, W. E. and Hughs, R. V.: "Directional Permeability Measurements and Their Significance," Producers Monthly (November, 1948) Vol. 13, No. 1, 17.

9. Kelton, F. C.: "Analysis of Fractured Limestone Cores," TRANS. AIME (1950) 189, 225-234.

10. Landrum, B. L. and Crawford, P. B.: "Effect of Directional Permeability on Sweep Efficiency and Production Capacity," TRANS. AIME (1960) 219, 407-411.

11. Lin, J.: "An Image Well Method For Bounding Arbitrary Reservoir Shapes in the Streamline Model," Ph.D. Dissertation, The University of Texas (December, 1972).

12. Mortada, M. and Nabor, G. W.: "An Approximate Method For Determining Areal Sweep Efficiency and Flow Capacity in Formations with Anisotropic Permeability," TRANS. AIME (1961) 222, II-277.

13. Muskat, M.: The Flow of Homogeneous Fluids Through Porous Media, McGraw-Hill Book Company, Inc. New York, N. Y. (1937).

14. Pettijohn, F. J.: Sedimentary Rocks, Harper and Row Publishers, New York, N. Y. (1957), 89.

15. Rinard, R. E.: "Analog Simulation of Anisotropic Permeability," M.S. Thesis, Louisiana State University (May, 1974).

16. "System/360 Scientific Subroutine Package", International Business Machines Corporation, White Plains, N. Y. (1968), 124, 125.

VITA

Louis Oved Chemin, Jr., the son of Betty Ray Miller and Louis O. Chemin, was born June 6, 1949 in Baton Rouge, Louisiana. Upon graduating from Central High School, Baton Rouge, Louisiana in May of 1967, he entered Louisiana State University. In September of 1969 he resigned from the university to serve a full time two year mission in Europe for the Church of Jesus Christ of Latter-Day Saints. Upon completion of his mission in September 1971 he returned to Louisiana State University and received a Bachelor of Science degree in Petroleum Engineering in May of 1973. In September of 1973 he entered the Graduate School of Louisiana State University to pursue a Master of Science degree in Petroleum Engineering. On June 7, 1974 he married Marilyn Sue Wamsley of Baton Rouge, Louisiana. Upon graduation he plans to be employed by Tenneco Oil Company in Denver, Colorado.